Master's thesis

NTNU
Norwegian University of Science and Technology
Faculty of Economics and Management
Dept. of Industrial Economics and Technology Management

Curd Schade

The impact of electric vehicle charging schemes and battery degradation on energy supply costs for a local energy community

Master's thesis in Sustainable Energy Systems and Markets
Supervisor: Ruud Egging-Bratseth
June 2022

NTNU
Norwegian University of Science and Technology

Curd Schade

The impact of electric vehicle charging schemes and battery degradation on energy supply costs for a local energy community

Master's thesis in Sustainable Energy Systems and Markets
Supervisor: Ruud Egging-Bratseth
June 2022

Norwegian University of Science and Technology
Faculty of Economics and Management
Dept. of Industrial Economics and Technology Management

NTNU
Norwegian University of
Science and Technology

Preface

In August 2021, I came to Trondheim as a participant in the double-degree master program SESAM (Sustainable Energy Systems and Markets) at the NTNU and TU Berlin. A major part of the first semester in Trondheim is a project in preparation of the Master's Thesis. I was interested to investigate optimal charging strategies for electric vehicles in smart neighborhoods. As previous year SESAM student Clara Pfister had worked on analysing a building complex energy system, I could use her project work as a starting point. I want to thank Clara for the provided ground work and data. I extended her project *Minimization of energy supply costs for a smart building complex* with several electric vehicles to analyse how different charging strategies for an increasing number of electric vehicles may influence the operational energy costs of a local neighborhood. Additionally, discussions with my supervisor Ruud Egging-Bratseth sparked the idea to incorporate battery degradation costs in the work. The project showed the importance of battery degradation in operational decisions and costs, even though we only considered degradation rudimentary. For the Master's Thesis, Ruud and I decided to delve deeper into that topic. We decided to divide this thesis into two journal paper, where in the first we purely focus on battery degradation and the development of a scalable, accurate battery optimization model with the goal to incorporate such model into the work from the project. Furthermore, the second paper considers uncertainty in the optimization to grasp the full extend of additional flexibility within the energy system through electric vehicle charging schemes.

I want to thank you Ruud for the great study program and your challenging but very fruitful supervision throughout my year at NTNU. Further, I want to thank Parinaz for her helping hand in the stochastic part of the second paper.

Last but not least, I want to thank all the other students of SESAM. We have spent hours studying together, helping and learning from each other, next to the social time away from the campus. I could not have done this without you, thank you!

Abstract

Optimal energy management becomes increasingly important in the future energy system. The increasing share of intermittent energy sources, such as solar power, requires additional flexibility in the system to balance supply and demand. Batteries are a solution for this increasing need for flexibility. The majority of techno-economic models in the literature overly simplify the representation of battery degradation. Especially in dynamic and uncertain settings, accounting properly for battery degradation will allow for better cost-effective trade-offs and optimization of battery usage.

In the first part of this thesis, we propose scalable model formulations for battery degradation, considering the impact of Cycle Depth (CD) and the State of Charge (SOC) on calendar and cycle aging of the battery. We set up a simple price arbitrage model, where for given market prices, a model decides electricity trades, battery charges and discharges of electricity, to maximize profit. We investigate how a better representation of degradation affects charging and discharging patterns.

The results show the importance of an accurate representation of battery degradation. In a setup ignoring battery degradation, an ex-post calculation of degradation costs reveals hidden costs that exceed the revenues and hence turn what seem to be profitable trades into losing trades. We observe that considering battery degradation leads to smaller CDs and a lower average SOC. Overall we show that a much-improved representation of battery degradation is possible and that two of the three degradation mechanisms can be represented very well at a low computational cost.

In the second paper, we use the resulting degradation model in a stochastic model for an urban neighborhood to analyze the interplay between Electric Vehicle (EV) charging schemes and battery usage and degradation, and their impact on the energy costs of the local neighborhood.

We propose a model incorporating PV modules, a combined heat and power plant (CHP), a stationary battery, and multiple EVs. We first analyze the neighborhood in a deterministic setting to assess the impact of passive, smart, and vehicle-to-grid (V2G) charging strategies. Here we find that the smart charging is already sufficient in reducing the system costs and V2G charging provides no significant added benefits.

The final analysis concerns multistage stochastic cases in which we incorporate un-

certainty in electricity prices and arrival SOCs of the EVs. Here we find that the V2G charging scheme can cope much better with the uncertainty resulting in up to 2.1% reduction in total system costs with a switch from smart to V2G charging.

With these two papers, this thesis provides several contributions to the academic literature. First, we show that it is possible to reflect more than 90% of the actual battery degradation using functional forms that scale well in techno-economic mathematical programming models, including the economic dispatch of batteries.

Second, we compute how much otherwise *hidden* battery degradation costs can be and how relatively minor schedule adjustments can considerably mitigate the battery degradation.

Third, we analyze that the flexibility of smart charging strategies, i.e., allowing a model to choose the best times to charge rather than passive charging from the moment an electric vehicle is plugged in, provides a significant part of the benefits of a vehicle-to-grid strategy. However, the value of vehicle-to-grid becomes larger when uncertainty increases.

Fourth, based on our observations, we list conditions that are critical success factors for the profitability of vehicle-to-grid.

Table of Contents

1 Introduction

The recently published IPCC report [1] comes to the alarming result that the effects of climate change are already more perceptible than expected. However, greenhouse gas emissions are still increasing worldwide, so that we approach climate tipping points. Therefore, minimizing CO_2 emissions and reaching climate neutrality is vital. Hence, we need to become more sustainable in all areas of life. As part of the energy sector's decarbonization efforts, the share of Renewable Energy Sources (RES) is increasing to replace the conventional power generation based on fossil fuels.

However, RES are characterized by intermittency and uncertainty, which may affect the power grid's reliability. Energy storage can help manage these issues with their ability to shift energy through time. Characteristics such as high power and energy density, spatial placement flexibility, and fast response times combined in one technology favor batteries compared to other storage technologies like pumped hydro, compressed-air energy, or flywheels. [2] As a result of these characteristics, and considering a continuing decrease in battery costs [3], we expect a major increase in battery storage usage in the energy sector. Another related development is the rapid penetration of Electric Vehicles (EV) [1], which with their electric battery capacity, may also provide balancing services. Vehicle-to-Grid (V2G) services concern discharging EV batteries to support grid management by providing services such as frequency regulation, load flattening, and load balancing. [4]

Intensive usage of batteries accelerates their aging due to physical and chemical stresses leading to material degradation, reduced performance, and reduced safety of the battery [5, 6]. For EV batteries, it is generally accepted that a 20% reduction in rated capacity and, thereby, the driving range, implies their end of life. Batteries are an expensive technology, and battery replacement adds significant cost to a vehicle's usage costs.

Battery degradation itself should be minimized to maximize the battery lifetime. However, in a broader problem scope with, for example, very high and very low, or even negative electricity prices, minimizing battery degradation may mean charging at unfavorable prices and forgoing on opportunities to charge very cheaply. Arbitraging large price differences can allow for steep financial profits, however, at the expense of increased battery degradation. Therefore, economic dispatch models considering the dispatch of batteries should explicitly trade off profit opportunities and the added stress on the battery and the resulting degradation and reduced battery

life. This leads to the first two research questions of this thesis:

1. How does a detailed representation of battery degradation influence battery operation in an economic dispatch setting?
2. How can we balance more accurate scheduling decisions for batteries with the model scalability?

Through a literature research, we gather the main operational influences on battery lifetime and decide to include the Cycle Depth (CD), average cycle State of Charge (SOC) and SOC-based calendar aging influence on the battery life. We develop an extended battery degradation model for a simple arbitrage setting, expanding upon the CD-based degradation model developed in the master pre-project in the Fall of 2021. The review, model, and results are described in a journal paper. The main challenge in this first journal paper is the trade-off between model accuracy and scalability because battery degradation mechanisms show non-convex behavior.

Our results show that two out of three degradation mechanisms can be incorporated without significantly affecting model tractability. Furthermore, we show the importance of battery degradation as part of the model decision variables, as neglecting battery degradation can lead to overly aggressive battery scheduling. This results in seemingly profitable trades becoming unprofitable due to high degradation costs that are not accounted for. We also show that a CD-based model alone is insufficient for prolonging the battery lifetime. The addition of degradation in relation to the SOC leads to an on average lower resting SOC, which is especially beneficial for mitigating the calendar aging of a battery.

In a second journal paper, we integrate the developed degradation model in a broader setting. We consider a local energy community in Pfreimd, Germany, with multiple generation and demand sources. This community consists of four buildings connected through a local electricity and a local heat grid. Each building has PV modules installed. Moreover, each building is connected to an external electricity and district heat grid, and one building features a small-scale combined heat and power plant (CHP) and a thermal energy storage(TES). To reflect a potential future situation of interest, we add a stationary electric battery to the complex and EV charge stations on the parking lot. In this setting, there are many degrees of freedom, and hence optimizable decisions, in the interplay of different types of power and heat generation and storage equipment, and variations and uncertainty in demand and prices.

With this model setup, we address the following questions:

1. What is the impact of electric vehicle charging schemes on the operational energy costs of a neighborhood?

2. How do uncertainty and the accurate representation of battery degradation influence the optimal system behavior?

We address the first question by considering three different charging schemes, *passive*, *smart* and *V2G* charging. While passive charging includes no flexibility for EV charging, smart charging allows the system to optimize when to charge. The V2G charging scheme allows EV discharging to provide additional generation flexibility for the neighborhood.

The results indicate cost savings of more flexible charging schemes by up to 10% and EV battery degradation reduction by up to 29%. However, in the deterministic setting, we see no significant difference between *smart* and *V2G* charging schemes. This changes with the addition of uncertainty for electricity prices and EV charging load. Due to the increased flexibility, V2G allows the system to respond better to external changes. The V2G option results in 2.1% lower costs than smart charging under the same price and SOC conditions as in the deterministic case, and up to 3.3% in the highest price scenario.

The added flexibility of a V2G charging scheme will become increasingly beneficial in the future, as the increasing share of renewable production will lead to total market supply becoming more volatile, and thus electricity prices too.

2 Paper 1 - The impact of battery degradation on economic dispatch optimization

The impact of battery degradation on economic dispatch optimization

Curd Schade * †, Ruud Egging-Bratseth *,
* Norwegian University of Science and Technology, Dept. of Industrial Economics and Technology Management
† Technical University Berlin, Workgroup for Infrastructure Policy

***Abstract*—Optimal energy management becomes increasingly important in the future energy system. The increasing share of intermittent energy sources, such as solar power, requires additional flexibility in the system to balance supply and demand. Batteries are a solution for this increasing need for flexibility. However, we observe that virtually all techno-economic models in the literature overly simplify the representation of battery degradation. Especially in dynamic and uncertain settings, accounting properly for battery degradation will allow for better, cost-effective tradeoffs and optimal battery usage. However, the scalability of the resulting model formulations is a major issue. In this paper, we propose a scalable model formulation for battery degradation, considering the impact of Cycle Depth and the State of Charge on calendar and cycle aging of the battery. We develop piecewise linear functions for which we show high representative accuracy. We set up a simple price arbitrage model, where a model decides electricity trades, battery charges and discharges of electricity to maximize profit for given market prices. Finally, we investigate how a better representation of degradation affects charging and discharging patterns and how this improved accuracy affects computational time. The results show the importance of an accurate representation of battery degradation. In a setup ignoring battery degradation, an ex-post calculation of degradation costs reveals hidden costs that exceed the revenues and hence turn what seem to be profitable trades into losing trades. Furthermore, we observe that considering battery degradation leads to smaller Cycle Depths and lower average States of Charge. Overall we show that a much-improved representation of battery degradation is possible and that two of the three degradation mechanisms can be represented very well at a low computational cost.**

***Index Terms*—electric battery degradation, economic dispatch, cycle depth, state of charge, calendar aging**

NOMENCLATURE

C-rate	Current rate
CD	Cycle Depth
DOD	Depth of Discharge
EV	Electric vehicle
LFP	Lithium Iron Phosphate
NMC	Nickel Manganese Cobalt
PV	Photovoltaic
RES	Renewable Energy Sources
SOC	State of Charge
SEI	Solid–Electrolyte Interphase
V2G	Vehicle-to-Grid

Sets	
$h \in H$	Hours
$j \in J$	Battery segments
$i, m \in I$	Calendar aging breakpoints

Variables	
A_h^{cyc}	Auxiliary, deviation to 50% SOC
A_h^{st}	Auxiliary, SOC at cycle start
B_h^C	Binary, charge mode active
$B_{i,h}^{CAL}$	Binary, SOS2 variable
B_h^D	Binary, discharge mode active
B_h^{END}	Binary, end of a cycle
B_h^S	Binary, steady-state mode active
B_h^{St}	Binary, start of a cycle
$C_{j,h}$	Battery charge
$D_{j,h}$	Battery discharge
K_h	Cost of battery degradation
N	Number of segments
Q_h^{CAL}	Calendar aging based capacity loss [%]
Q_h^{CD}	Cycle depth based capacity loss [%]
Q_h^{SOC}	Average cycle SOC based capacity loss [%]
$S_{j,h}$	Storage Level variable
SOC_h	State of charge
$Z_{h,i}$	SOS2 weight factor

Parameter	
c^{max}	Maximum charge
d^{max}	Maximum discharge
e^{rated}	Rated energy of the battery
f	Fitting parameter for average SOC stress
p_h	Electricity price
R	Replacement cost of the battery [€/kWh]
v^c	Charging efficiency
v^d	Discharging efficiency
o_i^{CAL}	Calendar aging breakpoint
o_j^{CD}	CD Breakpoint
y_i	Calendar aging breakpoint aging value

I. INTRODUCTION

In the last decade, the share of Renewable Energy Sources (RES) in the energy mix is increasing globally. Particularly prominent are wind and Photovoltaic (PV) power. These technologies are characterized by intermittency and uncertainty, which may affect the power grid's reliability. Energy storage can help manage these issues with its ability to shift energy through time. Characteristics such as high power and energy density, spatial placement and size flexibility, and fast response times favor batteries compared to other storage technologies like pumped hydro, compressed-air energy, or flywheels [1]. As a result of these characteristics combined with a continuing decrease in battery costs [2], we expect a major increase in battery storage usage in the energy sector. A related development is the rapid penetration of Electric vehicles (EVs), which with their electric batteries, may also provide balancing services.

Vehicle-to-Grid (V2G) services concern discharging EV batteries to support grid management by providing services such as frequency regulation, load flattening, and load balancing. [3]

Intensive usage of batteries accelerates their aging due to physical and chemical stresses leading to material degradation, reduced performance, and reduced safety of the battery [4], [5]. For EV batteries, it is generally accepted that a 20% reduction in rated capacity and, thereby, the driving range, implies their end of life. Batteries are expensive, and battery replacement significantly adds to vehicle usage costs.

Battery degradation itself should be minimized to maximize the battery lifetime. However, in broader problem settings with, for example, very high and very low or even negative electricity prices, minimizing battery degradation may mean charging at unfavorable prices and forgoing on opportunities to charge very cheaply. Arbitraging large price differences can allow for steep financial profits, however, at the expense of increased battery degradation. Therefore, economic dispatch models considering the dispatch of batteries should explicitly trade off profit opportunities and the added stress on the battery and the resulting degradation and reduced battery life.

This paper firstly addresses the question: *How does a detailed representation of battery degradation influence battery operation in an economic dispatch setting?* Secondly, it considers the supporting question: *How can we balance more accurate scheduling decisions for batteries with the model scalability?*

First, we discuss battery structure and aging mechanisms and their relevance in economic dispatch modeling. Next, we propose an economic dispatch model with adequate functional forms for battery degradation, balancing technical representation accuracy with numerical tractability. Last, we test our model for accuracy in a market price arbitrage setting and assess the impact of the individual degradation mechanisms, including sensitivity analysis for battery replacement costs.

II. Literature

A Lithium-Ion battery consists of a carbonaceous anode, a metal oxide cathode, a lithium salt electrolyte, and a separator. Each of these four components experiences degradation, causing decreasing power output and reducing the maximum stored energy, which affects overall battery lifetime. Battery lifetime is related to a battery's purpose. Generally it means that the battery's capacity is reduced so much that it can no longer adequately perform its intended purposes.

Battery life has two components: the calendar life, and the cycle life. The aging behaviors are additive, so we should aim to minimize both [6], [7]. Calendar life corresponds to the time before the battery reaches a purpose-specific capacity threshold, e.g., 80% of the original capacity due to chemical decay, and is independent of how the battery is used. Cycle life is connected to the number of (charge and discharge) cycles a battery can experience before the battery reaches the end of life criterion (e.g., 80% capacity). In frequently used batteries, the cycle life is always the decisive lifetime component [8]. Stationary batteries connected to electricity grids are often frequently used, hence, cycle life is generally decisive for the life of stationary batteries. In contrast, EV batteries are idle for large parts of the day, and typically have few cycles per day; therefore for EV batteries calendar aging is generally the dominant influence.

A. Calendar degradation mechanisms

Calendar aging is mostly driven by time, ambient temperature, and the State of Charge (SOC). Time, and often ambient temperature, are uncontrollable, external parameters, while the SOC (and sometimes temperature) is affected by operational decisions [8]–[10]. Prolonged, very high SOC levels are devastating to batteries [9], [11]. In addition, measurements of SOC-induced stress indicate that there are *aging plateaus* in the stress curves; local areas where modest changes in SOC hardly affect stress, and accelerating aging sections at other SOC levels [7].

Most batteries operate optimally at a cell temperature of approximately 25°C [4]. While the cell temperature has a very significant impact, with about doubled battery aging for every 10°C - 15°C increase, it is an easily and cheaply controllable parameter in stationary conditions by using ventilation. Furthermore, it is difficult to assess the influence of the ambient temperature on cell temperature, as both temperatures can deviate significantly, especially for actively used batteries in low ambient temperature conditions. Therefore, temperature is often not considered in (techno-economic) optimization models [5], [12]–[14]. Finally, while low ambient temperatures are beneficial for the calendar lifetime, they can be harmful to the cycle lifetime [15].

B. Cycle degradation mechanisms

Besides the intended exchange of electrons, battery charging and discharging causes side reactions that cause battery degradation by increasing the internal resistance and reducing the storage capacity. Physical (or mechanical) aging refers to the loss of active material (e.g., lithium oxide) in the electrodes and is connected to operation decisions Cycle Depth (CD) and SOC. In contrast, chemical aging refers to the loss of lithium inventory for transport between electrodes and is mostly connected to the time, temperature and Current rate (C-rate) [4], [8]. Battery cycling induces physical stress in the form of volume changes through the intercalation and deintercalation of lithium ions in the anode and the cathode. These volume changes lead to particle fractures at the electrodes, thereby exposing additional electrode surface to the electrolyte, which leads to a growth of the Solid–Electrolyte Interphase (SEI) layer. This, in turn, results in a permanent drop in cell capacity and, thereby, in overall battery capacity [11].

Next we describe the four main cycling-related degradation drivers: CD, C-rate, temperature, and SOC.

Deeper discharge cycles result in faster battery aging [10], [16]. In the literature, the term Depth of Discharge (DOD) is used both for the absolute discharge level of the battery (such that SOC+DOD=100%), but also as a synonym for the depth of a battery discharge compared to a starting SOC different from 100%. To be clear, we only use DOD with the meaning

DOD=100%-SOC. For the other meaning we use Cycle Depth (CD). The following two definitions of CD are useful in the context of battery degradation [17]:

1) a full cycle consists of one discharging and one charging event with the same depth,
2) a half cycle consists of one charging or discharging event.

According to measurement results, operating a battery with 10% cycle depths compared to 100% cycle depths allows 100 times more cycles and, therefore, a ten times larger energy throughput [18]. This shows a pronounced non-linear relationship between CD and aging behavior of Lithium-Ion batteries, which is typically not accounted for in economic dispatch models.

The second important cycling related aging driver is the C-rate. It is defined as the charging or discharging current divided by the rated storage capacity of the battery [in Ah]. The charge and discharge voltage can be considered constant in grid applications, hence, we can express the C-rate relative to a full charge or discharge in one hour, Eq. (1) with, P as power, and e^{rated} as rated energy, the maximum stored energy. The constant voltage removes one variable, thereby enables a less complex modeling of the C-rate [1].

$$\text{C-rate} = \frac{P}{E_{rated}} \tag{1}$$

Then, 1C indicates a full battery charge in 1 hour, 2C represents a full charge in 30 minutes, and C/2 means a full charge in 2 hours. Lower C-rates generally results in lower battery aging [6]. Batteries live through three degradation phases. In phase one, representing the first cycles of a new battery, the aging is the most pronounced. This rapid aging correlates with the initial formation of the SEI layer resulting in up to 5% capacity loss. In the second phase, the battery is more stable, aging more slowly compared to the other phases. With moderate C-rates, the battery spends the most number of cycles in this stage. After approximately 12% capacity loss (including phase one), the battery enters phase three, in which we see an increased sensitivity toward the C-rate. Hence, reducing battery degradation not only prolongs battery life directly, but also indirectly, by keeping the battery longer in phase two.

While low C-rates are generally advisable for battery longevity, the discharge efficiency in low-temperature conditions is worse with low discharge rates. This is attributed to a lower solid-state diffusivity of the Li-ions and a low ionic conductivity of the electrolyte, as well as a much higher interfacial charge transfer resistance [19]. Therefore, optimal battery operation strategies will vary depending on the ambient temperature. Generally, C-rates below 1C have modest impact on battery capacity, regardless of the battery type [8], [20]. However, the impact of higher C-rates varies greatly with the battery chemistry. While values over 1C cause significant damage to Nickel Manganese Cobalt (NMC) batteries, Lithium Iron Phosphate (LFP) batteries are less affected up to 4C. Considering EVs, a C-rate of 1C will hardly ever be surpassed, even in rapid charge mode, due to the battery management system [21]. For grid applications, the power rating is often lower than the energy rating of the battery, which makes C-rates exceeding 1C physically not possible. Consequently, in these situations, the C-rate only has a modest influence on the battery degradation and can be ignored when modeling batteries with a low power rating. In contrast, for battery use in high-power applications such as frequency regulation, the C-rate impact can be high and should be considered in modeling approaches [1].

The third important cycling-related aging driver is the cell temperature. High cell temperatures accelerate chemical reactions and thus harmful side reactions. As discussed in Section II-A above, the ambient temperature sets the ground level for the cell temperature. The temperature gradient in the battery depends primarily on the C-rate: high C-rates will result in a high cell temperature. Therefore, the ambient temperature and the C-rate together set the cell temperature. Hence the combination of both should be used to determine the effect on cycle degradation.

Finally, while the SOC is often only considered as a driver for calendar aging, it also affects the cycle aging. The optimal average SOC for battery cycling is 50%, which means that cycles passing symmetrically through a SOC=50% cause least damage. (C.f., Figure 6 in the Appendix shows how degradation increases towards the extreme values SOC 0% and 100% [16], [22])

Table II shows how different the impact of individual parameters can be, based on the battery chemistry. NMC and LFP are the most common battery chemistries today, with NMC being more favored in EVs.

TABLE II: Impact of cycle aging factors for two common battery chemistries. Based on [22]

	NMC	LFP
CD	++++	+
Cell temperature	++++	++
Charge rate	++	++
Discharge rate	++	++++
Mean SOC	+	+

The number of + signs indicates the impact on degradation, where ++++ is the most significant influence.

III. Battery Degradation Modeling

Battery degradation mechanisms often have complex non-linear or even non-convex behavior. This complexity makes integrating many existing battery degradation prediction models in economic dispatch models difficult in regard to tractability. Some studies consider battery degradation through static upper and lower boundaries for the SOC or limit the battery power [23], [24]. This simple solution sets artificial limits and thus would never allow extreme SOCs or CDs. Additionally, it typically leads in to high resting SOC and relatively deep cycles, which is harmful to the battery life [25].

A second approach is the use of empirical models. These tailor mathematical formulations to measurements of specific battery cells. The biggest drawback of this approach is that the resulting curvefits are only valid for the specific tested battery type [22], [26].

Finally, the third approach is an electrochemical model. While this has the highest validity, it becomes very complex,

due to non-linear and non-convex formulations. Therefore, it can not be applied for long time horizons and requires very detailed data, like the voltage, current level, internal resistance, and the representation of the entire electric battery circuit [27], [28].

As we focus on implementing a fast-solving degradation model in the context of economic dispatch *optimization* and not solely degradation prediction *simulation*, we concentrate on empirical modeling. Furthermore, we are only interested in modeling aging mechanisms tied to operational parameters, such as SOC, CD, and C-rate.

In the end, the total battery degradation is the sum of calendar and cycle aging and thus is expressed as [8], [28], [29]:

$$Q = Q^{calendar} + Q^{cycle} \tag{2}$$

A. Calendar degradation

Multiple studies approach calendar aging with curve fits based on the Arrhenius Law Eq. (3), with capacity fade percentage Q, Arrhenius constant A, activation Energy E^a, gas constant R, and temperature [28], [30], [31].

$$Q = A \cdot \exp\left(\frac{-E^a}{R \cdot T}\right) \tag{3}$$

However, out of the influencing parameter for calendar degradation, the only one under the influence of the operator is the SOC. Calendar aging increases with the time spent in high SOC areas. A curve fit connects the SOC to the capacity loss via fitting parameters. Multiple curve fits exist in the literature for LFP [30], [31] and NMC batteries [28], [32]. These are either linear or higher polynomial equations. However, linear fits disregard the aging plateaus mentioned in Section II-A [7]. Therefore, a more accurate approach is a piece-wise linear representation of calendar aging.

B. Cycle degradation

1) Cycle Depth (Depth of Discharge): A piecewise linear approach is also often adopted for degradation cost modelling based on CD [9], [33]–[38]. This approach penalizes discharges more than proportional to their CD. The base of this model is the material stress function, which connects the CD and capacity loss per cycle. Two approaches to this stress function exist. First, it can be based on an amplitude function for physical stress, Eq. (4) [9], [16]. Parameter A displays the maximum capacity loss per cycle for 100% CD, while m resembles the fatigue strength exponent.

$$Q^{CD}(CD) = A \cdot CD^{\frac{1}{m}} \tag{4}$$

Second, it can be based on the Arrhenius equation, with fitting parameter B and z as in Eq. (5). However, this results in a concave shape of the stress function, which is in contrast to the common convex shape in literature [34].

$$Q^{CD}(CD) = B \cdot \exp\left(\frac{-E_a}{R \cdot T}\right) \cdot (CD \cdot e^{rated})^z \tag{5}$$

This stress function is the input for the segmented cost function Eq. (6), in which R resembles the replacement cost in €$/kWh$, e^{rated} the overall battery capacity, and N the number of virtual battery segments [9]. However, we have seen multiple takes on this cost function in the literature. We implement Eq. (6) similar to [35], [36], as it results in an simpler implementation of further aging mechanisms.

$$k_j = e^{rated} \cdot R \cdot [Q^{CD}(\frac{j}{N}) - Q^{CD}(\frac{j-1}{N})] \tag{6}$$

Figure 1a shows the influence of the segment number on the approximation accuracy. We see that more than four segments improve the piecewise linear approximation accuracy of the stress function only marginal. However, in Fig. 1b we see that the number of segments matters when we look at the cost function. More segments lead to less distinct cost increases between the segments. Thus, we reduce abrupt borders between segments. Additionally, a fine-grained segmentation leads to more accurate counting of individual CDs and together this achieves a less staggered, more realistic dispatch profile. Nevertheless, more segments increase the computational requirements. The relative error is approximately 2% with 16 segments for a NMC battery cell [9] and 64 segments for a tested LFP cell [34]. We want to minimize this error further and implement a non-uniform segmentation. Therefore, we implement a piecewise linear search algorithm prior to the optimization to find the optimal breakpoints for the segment. [39]

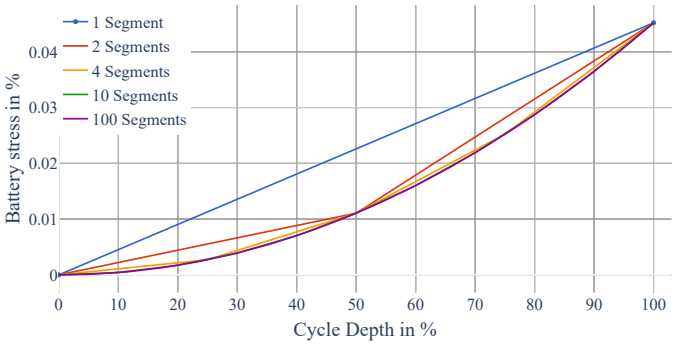

(a) Cycle degradation as a function of cycle depth

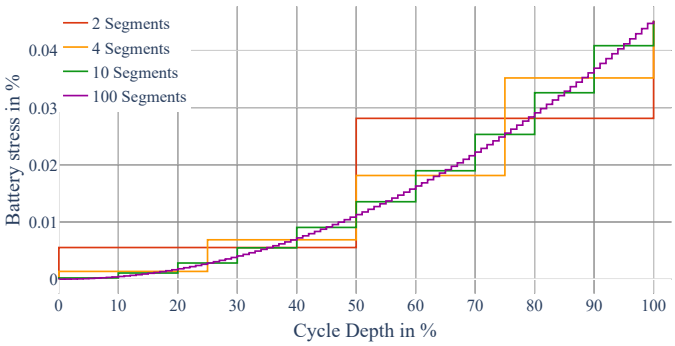

(b) Stepwise average cost increase per segment

Fig. 1: Battery Segmentation

2) Additional cycle degradation parameters: We see much less consideration of the C-rate based degradation. This is primarily due to the rather few high-power battery applications in the literature. Nevertheless, some studies consider the C-rate through a curve fit additionally to the CD model.

Additional approaches sum [8] or multiply [22] the individual degradation parameters, depending on the overall formulation approach. However, also entirely C-rate based models exist for high power applications [1]. Eq. (7) is then used as single influencing parameter, with β, δ, ζ, ω as fitting coefficients and C as C-rate.

$$Q^{loss} = \beta \cdot \exp\left(\delta \cdot C + \zeta\right) + \omega \tag{7}$$

However, as we mention in Section II-B, the C-rate is the main driver for temperature increase in a battery, while the ambient temperature sets the ground level for the cell temperature. Therefore, we can neglect the C-rate and the ambient temperature in the model under the assumption of using a high energy – e.g. low power battery – leading to overall low C-rates, and a constant ambient temperature of 25°C.

IV. Model Formulation

Eq. (8) is the objective function of the model, in which we minimize the battery degradation cost K over all timesteps. At the same time, we maximize the arbitrage value, from charges at low prices (purchases) and discharges at high price (sales) of the battery (Eq. (8)).

$$\text{MIN:} \sum_h (K_h - (p_h \cdot \sum_j (D_{j,h} - C_{j,h}))) \tag{8}$$

The objective function is subject to several constraints. These constraints are separated into battery and degradation constraints.

A. Battery balance Constraints

Eq. (9) computes the storage level at the start of each time step as the previous storage level modified by loss-corrected charges or discharges in previous time step. We propose a non-uniform virtual segmentation for the Q^{CD} formulation (Eq. (16)). Therefore, we multiply the rated energy e^{rated} with the length of each segment, where o_j^{CD} is the SOC value of the segment breakpoint, to establish the segment storage limit. Finally, Eqs. (11) and (12) restrict charges and discharges to their maximum values.

$$S_{j,h} = S_{j,h-1} + v^c \cdot C_{j,h-1} - \frac{D_{j,h-1}}{v^d} \qquad \forall\ j,h \tag{9}$$

$$S_{j,h} \leq e_{rated} \cdot (o_{j+1}^{CD} - o_j^{CD}) \qquad \forall\ j,h \tag{10}$$

$$\sum_j C_{j,h} \leq c^{max} \cdot B_h^C \qquad \forall\ j,h \tag{11}$$

$$\sum_j D_{j,h} \leq d^{max} \cdot B_h^D \qquad \forall\ j,h \tag{12}$$

$$B_h^S \geq 1 - \sum_j (D_{j,h} + C_{j,h}) \qquad \forall\ j,h \tag{13}$$

$$B_h^C + B_h^D + B_h^S = 1 \qquad \forall\ h \tag{14}$$

Furthermore, we define binary variables for three mutually exclusive battery modes –charging, discharging and steady state– in order to calculate the battery degradation (Eqs. (11) to (14)).

B. Battery degradation

We adopt the widely used CD and Rainflow Algorithm based model. Additionally, we consider the influence of the SOC on calendar aging and cycle aging. Thus the final model considers the capacity loss from three aging parameters: CD, average cycling SOC and SOC based calendar aging.

The degradation costs K consist of the individual capacity losses Q in % of each mechanism multiplied with the replacement cost R in €/kWh and e^{rated} in kWh.

$$K_h = R \cdot e^{rated} \cdot (Q_h^{CD} + Q_h^{SOC} + Q_h^{CAL}) \qquad \forall\ h \tag{15}$$

1) Cycle depth based degradation: For this degradation mechanism, it is important to account for small cycles within one overarching cycle. For example, a battery discharges from 100% to 40% SOC, causing major battery degradation. Afterward it charges up to 50% and down to 40% again, which causes only minor additional damage because the individual cycle only has a depth of 10%. Each discharge beyond the preceding deepest depth however damages the battery significantly. We keep track of the CD over the entire optimization period with the virtual segmentation of the battery. Eq. (16) imposes the CD based capacity loss, with j as the currently used segment, to localize the CD during discharging. We linearize the stress level of segment j with the breakpoints o_j^{CD}. The first term locates which segments, and how much of them are discharged in the current timestep, while the second term assigns the segments degradation.

$\forall\ h, j$:

$$Q_h^{CD} = \sum_j \left(\frac{D_{j,h}}{e^{rated} \cdot (o_{j+1}^{CD} - o_j^{CD})} \cdot \left[Q^{CD}(o_{j+1}^{CD}) - Q^{CD}(o_j^{CD}) \right] \right) \tag{16}$$

2) Average cycle SOC degradation: For this type of degradation we introduce several auxiliary values to keep track of battery cycles and crucial SOC levels. These are used to apply a penalty at the end of a discharge cycle. Eq. (17) computes the SOC at the end of every hour.

$$SOC_h = \frac{\sum_j S_{j,h}}{e^{rated}} \qquad \forall\ h \tag{17}$$

In the following Eqs. (18) to (20) and Eqs. (21) to (23) we formulate two binary variables that determine a start and end point of individual discharging half cycles. E.g., a cycle only starts when the battery did not discharge in $h-1$ and discharges in h. Further, Eq. (19) disables the start of a cycle if the battery already discharged in $h-1$. Eq. (20) restricts the start of a discharging cycle to h in which the battery is discharging. Vice versa, we compute in Eq. (21) the cycle end when the battery was in discharging mode in $h-1$ but is not discharging in the current timestep. This computes the cycle end one timestep later than the last discharge. Therefore, it can occur that a cycle at the end of the time horizon is not correctly computed when a discharge occurs in the last timestep. However, setting the discharge binary in the last timestep to zero, thereby disallowing discharging, solves this issue.

$$B_h^{st} \geq B_h^d - B_{h-1}^d \qquad \forall\ h \quad (18)$$
$$B_h^{st} \leq 1 - B_{h-1}^d \qquad \forall\ h \quad (19)$$
$$B_h^{st} \leq B_h^d \qquad \forall\ h \quad (20)$$
$$B_h^{END} \geq B_{h-1}^d - B_h^d \qquad \forall\ h \quad (21)$$
$$B_h^{END} \leq B_{h-1}^d \qquad \forall\ h \quad (22)$$
$$B_h^{END} \leq 1 - B_h^d \qquad \forall\ h \quad (23)$$

We use B_h^{st} in Eq. (24) to save the starting SOC of a cycle in the auxiliary variable A_h^{st}. In the following timesteps, the first term becomes zero. Hence, the second term copies the variable value of the previous timestep as long as the cycle continues. In order to reset A^{st} for the next cycle, we include B_{h-1}^{END} in the second term. Thereby, A_h^{st} always becomes zero if a cycle ended in the previous timestep, as the sum of the parenthesis becomes zero.

$$A_h^{st} = SOC_h \cdot B_h^{st} + (1 - B_h^{st} - B_{h-1}^{END}) \cdot A_{h-1}^{st} \qquad \forall\ h \quad (24)$$

Eqs. (25) and (26) use A_h^{st} to compute the deviation of the average SOC to 50%. Both equations are substitutes for an absolute function, which allows to save positive and negative deviations in the same variable. All variables are restricted to positive values, hence, Eq. (25) accounts for all deviations above 50% and Eq. (26) for all deviations below 50%.

$$A_h^{cyc} \geq \frac{SOC_h + A_h^{st}}{2} - \frac{1}{2} \qquad \forall\ h \quad (25)$$
$$A_h^{cyc} \geq \frac{1}{2} - \frac{SOC_h + A_h^{st}}{2} \qquad \forall\ h \quad (26)$$

Finally, in Eq. (27) we penalize the absolute deviation A^{cyc} with the penalty factor f. However, this penalty is only active at the end of each cycle. Thus we only penalize the average of a finished cycle and not continuously in every discharge period. Eqs. (24) and (27) are bi-linear constraints. The Gurobi solver can solve this type of constraints without further adjustments. However, if needed both constraints can be reformulated to linear constraints with McCormick envelopes.

$$Q_h^{SOC} = f \cdot A_h^{cyc} \cdot B_h^{END} \qquad \forall\ h \quad (27)$$

3) Calendar degradation: For the calendar life loss Q^{Cal} we use a piecewise linearization using SOS2 variables that define the active lincear segment. Eq. (28) computes the SOS2 weighting factor $Z_{i,h}$, thereby selecting the segment. Eq. (29) computes the calendar aging, according to the chosen segment. Eq. (30) ensures that the interpolation weights sum up to 1. Eq. (31) ensures only one segment can be active. Eq. (32) ensures that interpolation weights can only be positive for the active line segment.

$$SOC_h = \sum_i (o_i^{CAL} \cdot Z_{i,h}) \qquad \forall\ i,h \quad (28)$$
$$Q_h^{CAL} = \sum_i (y_i \cdot Z_{i,h}) \qquad \forall\ i,h \quad (29)$$
$$\sum_i Z_{i,h} = 1 \qquad \forall\ i,h \quad (30)$$
$$B_{i,h}^{CAL} + B_{h,m}^{CAL} \leq 1 \qquad \forall\ i, m > i+1, h \quad (31)$$
$$Z_{i,h} \leq B_{i,h}^{CAL} \qquad \forall\ i,h \quad (32)$$

V. Case Study

In the following section we test the model to assess the impact of the three considered degradation mechanisms. Furthermore, we conduct a sensitivity analysis on different battery replacement costs.

The optimization is set up in Pyomo and we use the Gurobi solver version 9.1.2 on a Intel(R) Core(TM) i5-6200U CPU @ 2.30 GHz processor with 8 GB RAM.

A. Input Parameters

We test the proposed model for a two day period from the 22^{nd} to 24^{th} of April 2019 with hourly timesteps. The prices are German spot prices [40], to which we add a grid fee of 7.39 ct [41] and a value-added tax of 19%. We chose a volatile price period because batteries offer their most value in these periods. However, the negative prices in the original time series are replaced by 0.1 ct/kWh. Otherwise, the negative price would negate the degradation cost completely due to profits through aggressive charging. Furthermore, we set the start and end SOC to zero.

TABLE III: Battery input parameters

Battery chemistry	NMC
Rated power	60 kW
Rated energy	100 kWh
Charge efficiency	95%
Discharge efficiency	95%
Assumed operating temperature	25°C
A in Eq. (4)	0.04519 %/cycle
m in Eq. (4)	0.4926
f	0.0085 %/cycle

Table III shows the battery parameters. We consider a NMC battery for all degradation parameters. Furthermore, the battery has a power to energy ratio of 0.6 (equal to the maximum C-rate). Further, we assume an operating temperature of 25°C; thereby eliminating the need for temperature consideration. The degradation parameter A, m, f are taken from a measurement series in [16] (c.f. appendix Fig. 6). For f we remove the offset caused by the cycle depth damage, to separate the impact of both mechanisms. We multiply the resulting maximum value by two, so that a deviation of 50% causes a damage of 0.00425%.

For the calendar degradation, we break down the ten-month NMC data for 25°C from [7] to hourly degradation values. However, as various studies have significantly lower degradation values, we adjust the parameters downwards with a factor of 0.25. Thus 100% SOC causes 2% capacity loss per year, which results in a ten-year shelf life of the battery for an end-of-life condition of 80% of the rated capacity [42]–[44]. Table IV shows the 5 chosen breakpoints, and Fig. 7 in the appendix presents the final piecewise linear function.

TABLE IV: Calendar aging values at segment breakpoints in $10^{-4}\%$

o^{CAL}	0%	30%	60%	70%	100%
y	1.50	3.50	4.0	7.43	8.93

B. Analysis

At first we asses the accuracy of the proposed model. Second, we analyze the impact of the individual degradation parameter. In both cases we use a replacement cost R = 150 €/kWh. Afterwards we conduct a sensitivity analysis for the replacement cost R.

1) Model accuracy: We measure the model accuracy with the relative error.

$$\text{relative error} = 100\% \cdot \frac{\text{calculated value} - \text{function value}}{\text{measured value}}$$

First, we compare the uniform segmentation and the optimized approximation approach. Therefore, we do a model run considering only Q^{CD} as degradation in the objective. Both approaches have very similar results with 5.000% error for uniform segmentation and 5.007% for the optimized approximation. This similarity is due to just minor adjustments to the breakpoints. In fact, the non-uniform segmentation performs slightly worse. We see in Fig. 2 that the breakpoints shift towards the upper end of the stress function. Thus the lower segments get bigger and less accurate, while the upper segments become smaller and more accurate. However, because the battery cycles more often in the smaller segments, the uniform segmentation performs better.

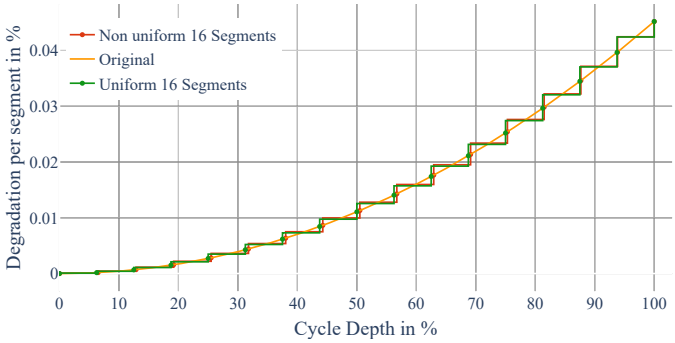

Fig. 2: Segmentation comparison

Now we run the model run with all degradation mechanisms active. At first, we notice in Table V that the relative error is positive, hence the model overestimates the degradation. This is expected as the piecewise linear segments are always above the real value for a convex function. For Q^{SOC}, the relative error is at 6.57%. Fig. 6, in the appendix, shows the original data which we used for the error calculation. Unfortunately, a quadratic curve deviates too much from the data for a reliable comparison. Therefore, we compare the model results to a piecewise linear function of the 5 data points of the original measurement.

Degradation mechanism	Relative error [%]
Combined degradation	3.32
Q^{CD}	3.24
Q^{SOC}	6.57
Q^{CAL}	1.62

TABLE V: Relative model error

Q^{CAL} is compared to a series of 16 points as seen in Fig. 7 in the appendix. We see a relative error of 1.62% for five breakpoints. Even better accuracy is achievable with an additional breakpoint at 90% SOC. However, in that case, the model solve time increases from 2 minutes to over an hour. Hence, we disregard that additional breakpoint to keep the model scalable. The total relative error for the degradation lies at 3.32%, which implies a very accurate model. However, we must notice that the comparison values stem from curve fits. Therefore, real verification through battery tests with the same scheduling is necessary.

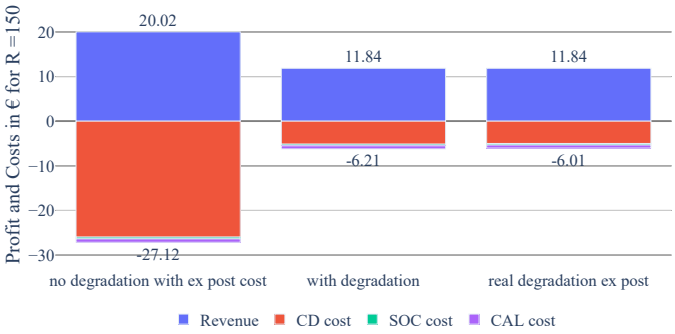

Fig. 3: Degradation cost vs. ex post cost calculation for R=150€/kWh

Finally, we see on the left bar of Fig. 3 that ex-post calculated degradation costs are higher than the revenues for a model run without degradation in the objective. This shows the importance of penalizing battery operation in the model. Without operational costs, the battery cycles to the full extent every time price differences create a small arbitrage opportunity even when the battery damage costs exceed the revenue. When degradation is considered, the battery revenue is cut by 40% but simultaneously, the degradation reduces significantly. Consequently, the battery now has a profitable operating schedule. Further, we see that the CD degradation costs seem to be the primary degradation factor. In the following section we analyze the individual impact of each degradation mechanism on the SOC profile of the battery.

2) Influence of degradation mechanisms: Fig. 4 shows the SOC over two days with different degradation mechanisms active in the optimization. The graphs for *no degradation* and *CAL* have almost the same SOC profile. We see very volatile cycles that exploit every price peak. This results in six cycles. Three of these cycles have a 100% CD, causing high battery degradation. At 00:00 on the second day, we observe a different schedule for *CAL* compared to *no degradation*. Despite a slight price increase, we see one hour delay for the charge. Thus the battery avoids one hour in 100% SOC, which lowers the calendar aging. Therefore, considering calendar aging can delay charges to limit the time spent in high SOC.

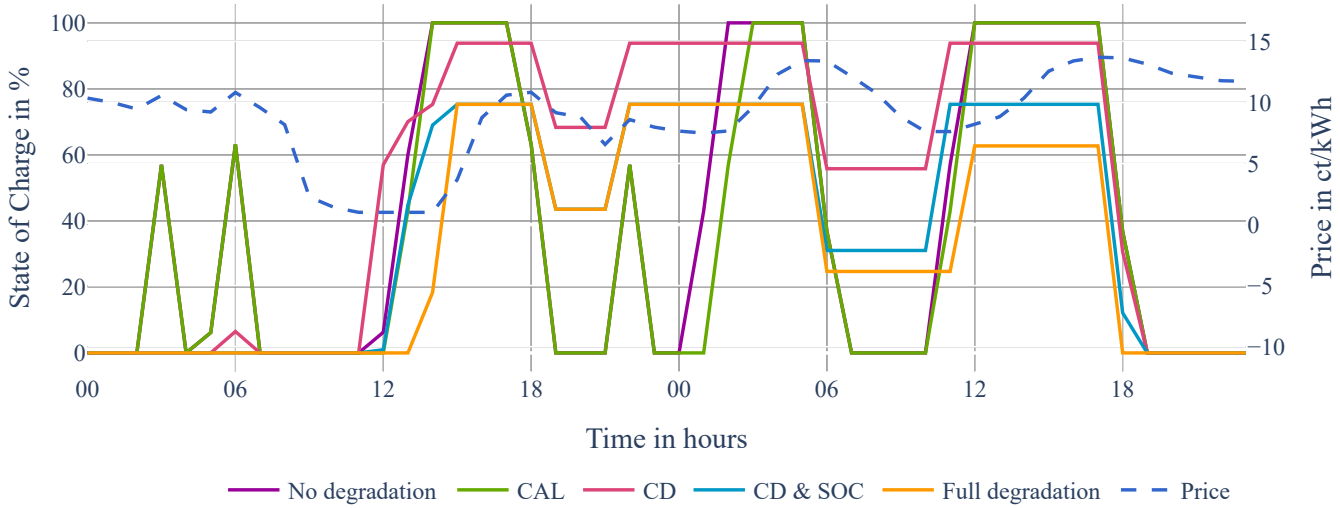

Fig. 4: SOC comparison for different degradation mechanisms considered in the model

Next, we look at the *CD* profile. At hour six of the first day, we observe the first difference from the previous profiles. One small 10% cycle replaces the two previous 60% cycles. We can trace that back to the small price difference at the charge and discharge hour. While the model previously exploits the full battery power, it uses significantly less due to added discharge costs that negate the previous revenues. Additionally, we observe entirely different battery behavior on the first day's evening. While the *no degradation* has a 100% discharge at 18:00, the battery now only discharges 25%. Thus significant aging of a 100% cycle is avoided. Furthermore, at midnight we see no discharge at all, as the price delta is rather small compared to the following hours. Similarly, we see a smaller discharge at 06:00. However, we still see a 100% discharge at 18:00. Despite significant battery aging, the model discharges because it is economically beneficial to go through a 100% cycle. The battery charges for free at 12:00 of the first day and now discharges for more than 13 ct/kWh. This shows the benefit of this cost-to-revenue trade-off approach instead of hard upper and lower boundaries. Hard boundaries would simply prevent full battery usage in this arbitrage situation.

Now we activate the full cycle degradation consisting of Q^{CD} and Q^{SOC}. At first, we notice that the small cycle at 06:00 of the first day is now gone. This is due to the cycling around an extremely low SOC during the *CD* run. Now, this additional battery stress is avoided. Furthermore, we see a lower average SOC in the next periods. The resting SOC until 18:00 is on 75% (blue line behind the yellow line) instead of 93% and we see a deeper discharge at 18:00 than before. While a deeper discharge causes slightly more CD related damage, it is a trade-off for a lower average SOC during cycling. Consequently, the addition of Q^{SOC} encourages deeper discharges above 50% starting SOC and discourages discharges below 50% starting SOC.

Finally, we see the interaction of all three mechanisms in the *full degradation* graph. For the first day, we see a similar SOC profile to the *CD & SOC* profile. However, due to active calendar aging, the model punishes high resting SOCs. Hence, the battery charges two hours later resulting in an overall lower average SOC. This becomes more pronounced starting 06:00 on the second day. Here we see a 50% discharge instead of the previous 40%. This has two effects. First, calendar aging is reduced as the battery goes down to 25% resting SOC. Secondly, Q^{SOC} is reduced to zero because the cycle starts at 75% and ends at 25% resulting in an average of 50%. Consequently, Q^{SOC} and Q^{CAL} have a complementary effect in this situation. Nevertheless, during the last charge period, we see the opposite. Here the calendar aging lowers the resting SOC, causing a higher Q^{SOC} during the last discharge. Finally, at 11:00, we see that the active calendar degradation leads again to a later charge hour than considering only cycle degradation.

Overall, we can assess that the consideration of battery degradation in the model provides drastically different optimal solutions than without degradation. Furthermore, we see that considering only the CD can lead to high resting SOCs and cycles at the higher and lower SOC spectrum. Thus it is advisable to consider multiple mechanisms. Additionally, we can prove the benefit of incorporating the degradation in the optimization instead of setting artificial SOC boundaries. This way, the battery is still fully usable in large arbitrage opportunities.

3) Sensitivity analysis on battery replacement cost: Fig. 5 shows SOC for a range of battery replacement costs with all three degradation mechanisms active. We set a price range from 50 to 500 €/kWh. This reflects the uncertainty in battery price forecasts. However, studies agree on decreasing prices for battery packs for the next decades [2]. Table VI shows performance indicators for the different battery price scenarios.

We observe that the average SOC decreases with rising R. This is due to higher calendar aging costs as well as more costly deep discharges. Thus the battery settles at 31% SOC for the highest price scenario, while we see 100% in the two lowest price scenarios. Furthermore, the cycle amplitudes are reduced and located closer to 50% SOC with increasing costs. The exception is $R = 500$, where the costs are so high that

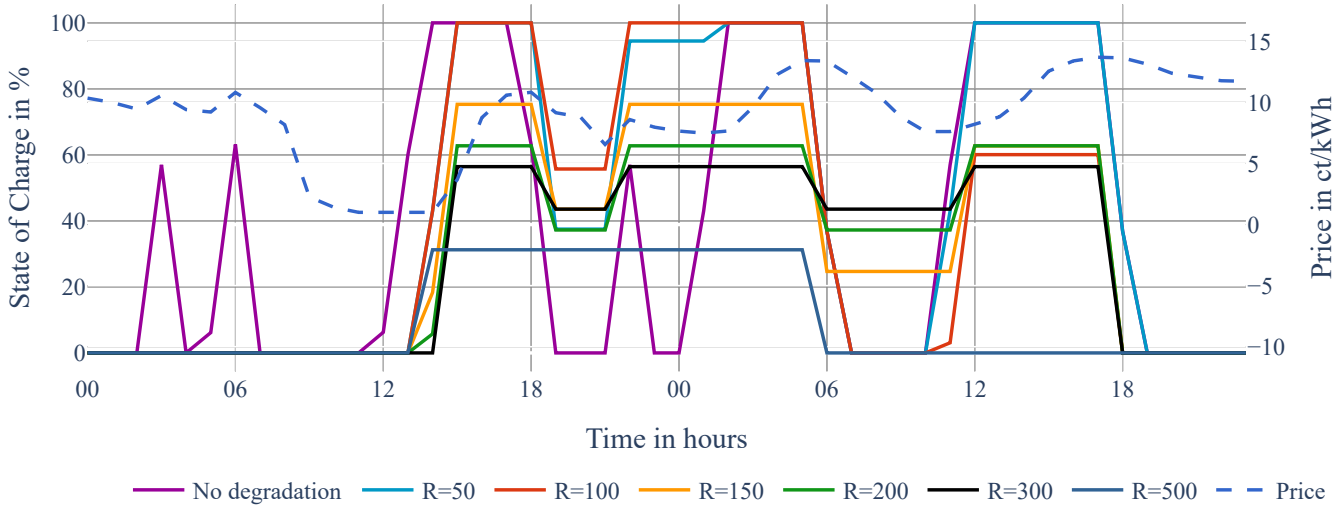

Fig. 5: Sensitivity analysis on R

the battery never charges beyond 31%. More distance to 50% SOC and thus a higher Q^{SOC} is the trade-off for lower Q^{CD} and Q^{CAL} in this case.

The annualized CD degradation value for $R = 50$ and $R = 100$ are at 18.7% and at 12.1%. This clearly shows the advantage of degradation costs as part of the optimization instead of hard SOC or CD boundaries. Damaging battery behavior is acceptable as the replacement costs are lower than the generated revenues.

Additionally, we see that the CD degradation has the dominating share of the total degradation throughout all prices. However, this gets less pronounced with increasing battery costs. In return, this means that Q^{SOC} and Q^{CAL} become more relevant. However, for Q^{SOC}, we see no clear trend as it depends on where the cycles occur. Thus we see a lower value for $R = 50$ because the battery has more 100% cycles, averaging at 50% compared to $R = 100$ where the SOC is lower during the second day.

Finally, the annualized profits show extensive arbitrage opportunities. Nevertheless, naturally, the profit decreases with rising battery costs. At $R = 500$, we observe higher costs than revenues, resulting in losses despite an optimal arbitrage setting. Consequently, the battery investment could hardly ever become profitable due to the high operational costs.

4) Model runtime: In addition, we want to address the model complexity and runtime in relation to the model accuracy. We see in Table VI that the contribution of each mechanism to the total battery degradation is very different. In the case of multiple and deep cycles, such as $R = 50$, we see that the CD degradation has a share of 93.5% of the total degradation, while the Q^{CAL} contributes 5% and Q^{SOC} only 1.5%. In the moderate and most realistic case of $R = 150$ this changes to Q^{CD} contributing 83.1%, Q^{CAL} contributing 11.1% and Q^{SOC} contributing 5.8%. Therefore, we see a clear priority of considering Q^{CD} in the optimization over the two other mechanisms. The model takes 5 minutes 46 seconds to solve the full degradation run for $R = 150$. Given that Q^{CD} has the most impact, we remove only Q^{SOC} and Q^{CAL} respectively from the model to assess the runtime influence of the added mechanisms. The combination of Q^{CD} and Q^{SOC} solves in 17 seconds, while the combination of Q^{CD} and Q^{CAL} solves in 0.87 seconds. Therefore, Q^{SOC} has the least impact on the model accuracy but by far the biggest influence on the run time. Furthermore, we assume that the model run time will not scale linearly due to the bilinear constraints Eqs. (24) and (27) and the number of binary variables. Consequently, we expect tractability issues for a larger number of timesteps and in stochastic settings, in which case we recommend removing Q^{SOC} from the optimization. This reduces the runtime considerably while maintaining a high model accuracy.

TABLE VI: Battery performance

KPI	Unit	R = 50	R = 100	R = 150	R = 200	R = 300	R = 500
Total charge throughput	[kWh]	249.38	194.13	137.87	108.07	78.08	29.69
Max SOC	[%]	100.00	100.00	75.32	62.75	56.44	31.25
Average SOC	[%]	42.71	37.72	32.86	30.64	29.33	10.42
Max CD	[%]	60.00	60.00	59.58	59.61	53.62	29.69
Annualized CD degradation	[%]	18.69	12.13	6.27	4.02	2.70	0.74
Annualized SOC degradation	[%]	0.29	0.75	0.44	0.29	0.34	0.27
Annualized CAL degradation	[%]	1.00	0.86	0.84	0.70	0.62	0.48
Annualized revenue	[€]	3415.63	2952.21	2161.41	1746.34	1421.5	666.72
Annualized degradation cost	[€]	999.17	1373.29	1132.51	1001.98	1098.08	742.15
Annualized profit	[€]	2416.46	1578.92	1028.9	744.35	323.42	-75.43

VI. Conclusion

This paper shows the importance of correctly representing battery costs for economic dispatch decisions. Out of multiple degradation mechanisms for lithium-ion batteries, we consider the cycle depth, average cycle SOC, and SOC-based calendar aging in a mixed-integer linear optimization model.

We can prove a good model accuracy of 3.3% relative error in relation to the input curve fits. However, a real test series for a battery adopting the operating schedule would provide further information about the model accuracy. We set out to improve the widely used rainflow approximation model with a non-uniform segmentation. However, the uniform segmentation performed slightly better.

Additionally, we prove the importance of correct degradation representation in optimizations. High price differences create considerable arbitrage opportunities for batteries. However, an ex-post calculation of degradation costs reveals that at first profitable trades result in losses, as aggressive battery scheduling leads to high hidden degradation costs. Additionally, commonly used hard SOC boundaries of 10-15% SOC as lower and 90% upper limit would prohibit these arbitrage situations. We show that the option for a trade-off between more damaging battery behavior and economically profitable scheduling is necessary. Furthermore, we see that the common CD model alone results in a high average cycle and resting SOCs, leading to higher cycle and calendar aging of the battery than accounted for in the model.

In the last step, we conduct a sensitivity analysis on the battery replacement cost. With increasing costs, we see lower cycle amplitudes, closer to 50% average cycle SOC. Furthermore, the battery becomes entirely unprofitable, even during high price differences, with a high replacement cost of 500 €/kWh.

Finally, we want to address the limitations of the proposed model and indicate further research possibilities. Our model has two core assumptions: 1) a stable 25°C operating temperature and 2) a C-rate lower than one. Thus we do not consider the effect of these parameters on the battery degradation. However, deviating temperatures and high C-rates result in additional battery stress that can even become the primary damaging influence. Thus the proposed model would lose accuracy. At last, the model needs to be tested in more advanced optimizations, as the goal is to incorporate the degradation model in general large-scale dispatch optimizations.

Appendix

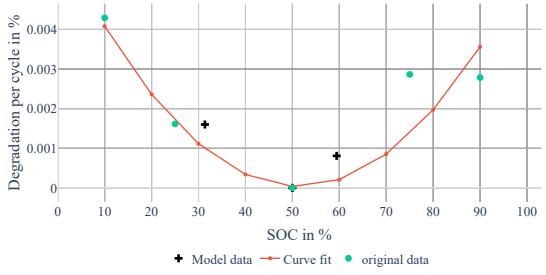

Fig. 6: Piecewise linear approximation of calendar aging

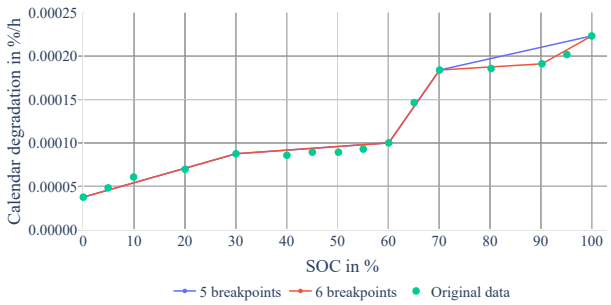

Fig. 7: Piecewise linear approximation of calendar aging, the sixth breakpoint is an additional at 90% SOC

References

[1] Z. Qiu, W. Zhang, S. Lu, *et al.*, "Charging rate based battery energy storage system model in wind farm and battery storage cooperation bidding problem," *CSEE Journal of Power and Energy Systems*, pp. 1–9, 2022.

[2] L. Mauler, F. Duffner, W. G. Zeier, and J. Leker, "Battery cost forecasting: A review of methods and results with an outlook to 2050," *Energy & Environmental Science*, 2021.

[3] Y. Amara-Ouali, Y. Goude, P. Massart, J.-M. Poggi, and H. Yan, "A review of electric vehicle load open data and models," *Energies*, vol. 14, no. 8, 2021, ISSN: 1996-1073.

[4] R. Xiong, Y. Pan, W. Shen, H. Li, and F. Sun, "Lithium-ion battery aging mechanisms and diagnosis method for automotive applications: Recent advances and perspectives," *Renewable and Sustainable Energy Reviews*, vol. 131, p. 110 048, 2020, ISSN: 1364-0321.

[5] X. Han, L. Lu, Y. Zheng, *et al.*, "A review on the key issues of the lithium ion battery degradation among the whole life cycle," *eTransportation*, vol. 1, p. 100 005, 2019, ISSN: 2590-1168.

[6] A. W. Thompson, "Economic implications of lithium ion battery degradation for vehicle-to-grid (v2x) services," *Journal of Power Sources*, vol. 396, pp. 691–709, 2018, ISSN: 0378-7753.

[7] P. Keil, S. F. Schuster, J. Wilhelm, *et al.*, "Calendar aging of lithium-ion batteries," *Journal of The Electrochemical Society*, vol. 163, no. 9, A1872–A1880, 2016.

[8] A. Ahmadian, M. Sedghi, A. Elkamel, M. Fowler, and M. Aliakbar Golkar, "Plug-in electric vehicle batteries degradation modeling for smart grid studies: Review, assessment and conceptual framework," *Renewable and Sustainable Energy Reviews*, vol. 81, pp. 2609–2624, 2018.

[9] B. Xu, J. Zhao, T. Zheng, E. Litvinov, and D. S. Kirschen, "Factoring the cycle aging cost of batteries participating in electricity markets," *IEEE Transactions on Power Systems*, vol. 33, no. 2, pp. 2248–2259, 2018. DOI: 10.1109/TPWRS.2017.2733339.

[10] C. Zhou, K. Qian, M. Allan, and W. Zhou, "Modeling of the cost of ev battery wear due to v2g application in power systems," *IEEE Transactions on Energy Conversion*, vol. 26, no. 4, 2011.

[11] J. S. Edge, S. O'Kane, R. Prosser, *et al.*, "Lithium ion battery degradation: What you need to know," *Phys. Chem. Chem. Phys.*, vol. 23, pp. 8200–8221, 14 2021.

[12] J. Chengquan, P. Wang, L. Goel, and Y. Xu, "A two-layer energy management system for microgrids with hybrid energy storage considering degradation costs," *IEEE Transactions on Smart Grid*, vol. 9, no. 6, pp. 6047–6057, 2018.

[13] C. Guenther, B. Schott, W. Hennings, P. Waldowski, and M. A. Danzer, "Model-based investigation of electric vehicle battery aging by means of vehicle-to-grid scenario simulations," *Jour-*

nal of Power Sources, vol. 239, pp. 604–610, 2013, ISSN: 0378-7753.

[14] J. Wang, P. Liu, J. Hicks-Garner, *et al.*, "Cycle-life model for graphite-lifepo4 cells," *Journal of Power Sources*, vol. 196, no. 8, pp. 3942–3948, 2011, ISSN: 0378-7753.

[15] D. Wang, J. Coignard, T. Zeng, C. Zhang, and S. Saxena, "Quantifying electric vehicle battery degradation from driving vs. vehicle-to-grid services," *Journal of Power Sources*, vol. 332, pp. 193–203, 2016, ISSN: 0378-7753.

[16] I. Laresgoiti, S. Käbitz, M. Ecker, and D. Sauer, "Modeling mechanical degradation in lithium ion batteries during cycling: Solid electrolyte interphase fracture," *Journal of Power Sources*, vol. 300, pp. 112–122, Dec. 2015.

[17] M. Koller, T. Borsche, A. Ulbig, and G. Andersson, "Defining a degradation cost function for optimal control of a battery energy storage system," in *2013 IEEE Grenoble Conference*, 2013, pp. 1–6.

[18] I. Baghdadi, O. Briat, J.-Y. Delétage, P. Gyan, and J.-M. Vinassa, "Lithium battery aging model based on dakin's degradation approach," *Journal of Power Sources*, vol. 325, pp. 273–285, 2016, ISSN: 0378-7753.

[19] W. Wu, W. Wu, X. Qiu, and S. Wang, "Low-temperature reversible capacity loss and aging mechanism in lithium-ion batteries for different discharge profiles," *International Journal of Energy Research*, vol. 43, no. 1, pp. 243–253, 2019.

[20] Y. Gao, J. Jiang, C. Zhang, W. Zhang, Z. Ma, and Y. Jiang, "Lithium-ion battery aging mechanisms and life model under different charging stresses," *Journal of Power Sources*, vol. 356, pp. 103–114, 2017, ISSN: 0378-7753.

[21] S. M. Bhagavathy, H. Budnitz, T. Schwanen, and M. McCulloch, "Impact of charging rates on electric vehicle battery life," *Findings*, p. 21 459, 2021.

[22] J. Olmos, I. Gandiaga, A. Saez-de-Ibarra, X. Larrea, T. Nieva, and I. Aizpuru, "Modelling the cycling degradation of li-ion batteries: Chemistry influenced stress factors," *Journal of Energy Storage*, vol. 40, p. 102 765, 2021, ISSN: 2352-152X.

[23] J. Yusuf and S. Ula, "A comprehensive optimization solution for buildings with distributed energy resources and v2g operation in smart grid applications," in *2020 IEEE Power Energy Society Innovative Smart Grid Technologies Conference (ISGT)*, 2020, pp. 1–5.

[24] M. Shakeri, M. Shayestegan, H. Abunima, *et al.*, "An intelligent system architecture in home energy management systems (hems) for efficient demand response in smart grid," *Energy and Buildings*, vol. 138, 2017.

[25] J. M. Reniers, G. Mulder, and D. A. Howey, "Unlocking extra value from grid batteries using advanced models," *Journal of Power Sources*, vol. 487, p. 229 355, 2021, ISSN: 0378-7753.

[26] A. J. Smith, P. Svens, M. Varini, G. Lindbergh, and R. W. Lindström, "Expanded in situ aging indicators for lithium-ion batteries with a blended NMC-LMO electrode cycled at sub-ambient temperature," *Journal of The Electrochemical Society*, vol. 168, no. 11, p. 110 530, Nov. 2021.

[27] J. M. Reniers, G. Mulder, S. Ober-Blöbaum, and D. A. Howey, "Improving optimal control of grid-connected lithium-ion batteries through more accurate battery and degradation modelling," *Journal of Power Sources*, vol. 379, pp. 91–102, 2018, ISSN: 0378-7753.

[28] T. M. N. Bui, M. Sheikh, T. Q. Dinh, A. Gupta, D. W. Widanalage, and J. Marco, "A study of reduced battery degradation through state-of-charge pre-conditioning for vehicle-to-grid operations," *IEEE Access*, vol. 9, pp. 155 871–155 896, 2021.

[29] M. Naumann, F. B. Spingler, and A. Jossen, "Analysis and modeling of cycle aging of a commercial lifepo4/graphite cell," *Journal of Power Sources*, vol. 451, p. 227 666, 2020, ISSN: 0378-7753.

[30] E. Sarasketa-Zabala, I. Gandiaga, L. Rodriguez-Martinez, and I. Villarreal, "Calendar ageing analysis of a lifepo4/graphite cell with dynamic model validations: Towards realistic lifetime predictions," *Journal of Power Sources*, vol. 272, pp. 45–57, 2014, ISSN: 0378-7753.

[31] U. Mulleriyawage and W. Shen, "Optimally sizing of battery energy storage capacity by operational optimization of residential pv-battery systems: An australian household case study," *Renewable Energy*, vol. 160, pp. 852–864, 2020, ISSN: 0960-1481.

[32] J. de Hoog, J.-M. Timmermans, D. Ioan-Stroe, *et al.*, "Combined cycling and calendar capacity fade modeling of a nickel-manganese-cobalt oxide cell with real-life profile validation," *Applied Energy*, vol. 200, pp. 47–61, 2017, ISSN: 0306-2619.

[33] S. Bjarghov, M. Kalantar-Neyestanaki, R. Cherkaoui, and H. Farahmand, "Battery Degradation-Aware Congestion Management in Local Flexibility Markets," in *2021 IEEE Madrid PowerTech*, 2021, pp. 1–6.

[34] L. Zhang, Y. Yu, B. Li, *et al.*, "Improved cycle aging cost model for battery energy storage systems considering more accurate battery life degradation," *IEEE Access*, vol. 10, pp. 297–307, 2022.

[35] Y. Shi, B. Xu, Y. Tan, D. Kirschen, and B. Zhang, "Optimal battery control under cycle aging mechanisms in pay for performance settings," *IEEE Transactions on Automatic Control*, vol. 64, no. 6, pp. 2324–2339, 2019.

[36] R. K. Bansal, P. You, D. F. Gayme, and E. Mallada, "Storage degradation aware economic dispatch," in *2021 American Control Conference (ACC)*, 2021, pp. 589–595.

[37] Y. Shi, B. Xu, Y. Tan, and B. Zhang, "A convex cycle-based degradation model for battery energy storage planning and operation," in *2018 Annual American Control Conference (ACC)*, 2018, pp. 4590–4596.

[38] S. Upadhya and M. J. Wagner, "A Dispatch Optimization Model for Hybrid Renewable and Battery Systems Incorporating a Battery Degradation Model," *Journal of Energy Resources Technology*, vol. 144, no. 7, Dec. 2021, 070907, ISSN: 0195-0738.

[39] A. Imamoto and B. Tang, "A recursive descent algorithm for finding the optimal minimax piecewise linear approximation of convex functions," *Lecture Notes in Engineering and Computer Science*, vol. 2173, Oct. 2008.

[40] Bundesnetzagentur. (2019), [Online]. Available: https://www.smard.de/home/downloadcenter.

[41] "Electricity price." (2019), [Online]. Available: https://strom-report.de/strompreise/#strompreiszusammensetzung.

[42] B. Rumberg, B. Epding, I. Stradtmann, M. Schleder, and A. Kwade, "Holistic calendar aging model parametrization concept for lifetime prediction of graphite/nmc lithium-ion cells," *Journal of Energy Storage*, vol. 30, p. 101 510, 2020, ISSN: 2352-152X.

[43] A. Krupp, R. Beckmann, T. Diekmann, E. Ferg, F. Schuldt, and C. Agert, "Calendar aging model for lithium-ion batteries considering the influence of cell characterization," *Journal of Energy Storage*, vol. 45, p. 103 506, 2022, ISSN: 2352-152X.

[44] B. Xu, A. Oudalov, A. Ulbig, G. Andersson, and D. S. Kirschen, "Modeling of lithium-ion battery degradation for cell life assessment," *IEEE Transactions on Smart Grid*, vol. 9, no. 2, pp. 1131–1140, 2018.

3 Paper 2 - Least cost vehicle charging in a smart neighborhood considering uncertainty and battery degradation

Manuscript to be submitted in IEEE Transactions on Smart Grid

Least cost vehicle charging in a smart neighborhood considering uncertainty and battery degradation.

Curd Schade*†, Parinaz Aliasghari*, Ruud Egging-Bratseth*, Clara Pfister*†
*Norwegian University of Science and Technology, Dept. of Industrial Economics and Technology Management
†Technical University Berlin, Workgroup for Infrastructure Policy

***Abstract*—The transition to a sustainable energy system leads to increasing supply by intermittent, distributed generation, while at the same time electrification and penetration of electric vehicles lead to higher, more variable and more uncertain demand. It is increasingly more interesting for neighborhoods to manage local supply and demand to minimize overall energy costs. The main options for this are storage technologies and demand response. In this study we assess the impact of different charging strategies for electric vehicles on the energy costs of a local neighborhood. We analyze a building complex incorporating solar PV modules, a small-scale combined heat and power plant, a stationary battery and multiple electric vehicles. We account for battery degradation to allow for cost-effective tradeoffs and increased optimization of battery usage. We reflect uncertainty in intraday prices, and user behavior via the electrical vehicle charging needs in a multistage stochastic approach.**

We discuss a deterministic case to illustrate the workings of the model. The stochastic results show a significant reduction of expected energy costs by up to 10% through flexible charging and a particular vehicle-to-grid benefit in an uncertain setting; the EV battery degradation is reduced by up to 30%.

***Index Terms*—battery degradation modeling, economic dispatch, energy storage, distributed energy resources**

ABBREVIATIONS

CHP	Combined Heat and Power plant
CD	Cycle Depth
DR	Demand Response
DG	Distributed Generation
EV	Electric vehicle
MG	Micro Grid
MILP	Mixed-Integer-Linear-Programming
NLP	Non-Linear-Programming
PV	Photovoltaic
RES	Renewable Energy Sources
SOC	State of Charge
TES	Thermal energy storage
V2G	Vehicle-to-Grid

NOMENCLATURE

Sets and indices	
$b \in B$	Buildings
$e \in E$	Energy carriers el, ht, gs
$h \in H$	Stochastic scenario tree nodes
$\tilde{h} \in H$	Predecessor scenario node of h
$\hat{h} \in H$	Terminal nodes of scenarios
$h^{arr} \in H$	Arrival time of EV
$h^{dep} \in H$	Departure time of EV
$i, m \in I$	Calendar aging breakpoints
$j \in J$	Segments in the battery
$L, M \in N$	Grid types n, local and main
$t \in T$	Generation technologies
$u \in U$	CHP breakpoints
$w \in W$	Storages

Variables	
$A^{St}_{b,w,el,h}$	SOC-level at cycle start
$A^{cyc}_{b,w,el,h}$	Deviation to 50% SOC
$B^{C}_{b,w,e,h}$	Binary, charge mode active
$B^{CAL}_{b,w,el,i,h}$	Binary, SOS2 calendar aging
$B^{CHP}_{u,h}$	Binary, SOS2 CHP operation
$B^{D}_{b,w,e,h}$	Binary, discharge mode active
$B^{END}_{b,w,el,h}$	Binary, end of a discharge cycle
$B^{S}_{b,w,e,h}$	Binary, battery steady-state
$B^{St}_{b,w,el,h}$	Binary, start of a discharge cycle
$C_{b,w,e,j,h}$	Battery charge
$CHP^{in}_{b,h}$	CHP gas consumption
$CHP^{out}_{b,e,h}$	CHP energy output
$CU_{b,e,h}$	Generation curtailment
$D_{b,w,e,j,h}$	Discharge
$G_{b,e,n,h}$	Grid extractions
$I_{b,e,n,h}$	Grid injections
$I^{CHP}_{b,e,M,h}$	Grid Injections, share of CHP
$I^{RES}_{b,e,M,h}$	Grid injections, share of RES
$K_{b,w,el,h}$	Collected cost of battery degradation
$Q^{CAL}_{b,w,el,h}$	Calendar aging based capacity loss [%]
$Q^{CD}_{b,w,el,h}$	Cycle depth based capacity loss [%]
$Q^{SOC}_{b,w,el,h}$	Average cycle SOC based capacity loss [%]
$S_{b,w,e,j,h}$	Storage Level
$SOC_{b,w,el,h}$	State of charge [%]
$X_{u,h}$	SOS2 weight factor for CHP
$Z_{b,w,el,i,h}$	SOS2 weight factor for calendar aging

Parameters	
$a_{b,w,h}$	EV availability
α_h	Scenario probability
$c^{max}_{b,w,e}$	Maximum charge
$d^{max}_{b,w,e}$	Maximum discharge
$dem_{b,e,h}$	Residential demand
$e^{rated}_{b,w,e}$	Rated energy of the storage
f	Fitting parameter for average SOC stress
$g^{RES}_{b,t,e,h}$	Renewable energy production
k^{end}	End of horizon penalty cost parameter for EVs
k^{O}	Operational costs of CHP
ntc_e	Net transfer capacity
$p_{e,h}$	Grid import price
p^{RES}	Price per kWh for RES feed in
p^{CHP}	Price per kWh for CHP feed in
R	Replacement cost of the battery [€/kWh]
$o^{CAL}_{b,w,i,h}$	Calendar aging breakpoint
$o^{CHP}_{u,e}$	CHP breakpoints
$v^{c}_{b,w,e}$	Charging efficiency
$v^{d}_{b,w,e}$	Discharging efficiency
$v_{e,n}$	Grid losses

$y_{b,w,i}$	Calendar aging breakpoint aging value

I. Introduction

Electricity distribution is becoming increasingly complex due to an progressively larger variety of consumption types –e.g. electric vehicles– with high demand peaks, and a rising share of decentralized Renewable Energy Sources (RES) feeding into the local distribution grids. [1], [2] The applicability of RES such as solar PV as the sole power generation source in urban settings is generally limited due to the fluctuating nature of its electricity generation [3]. Therefore, we need a smart set up and operation of energy systems. A straightforward solution to manage RES intermittency is by using storage units. Additionally, coupling the electricity grid and heat sector may help balance generation peaks and ease the integration of RES. Storage units for power and for heat have high unit investment costs, and, especially for electric batteries, charging and discharging patterns have a major impact on battery degradation, and hence lifetime. An optimal use of storage capacity allows for investing in smaller, hence cheaper, units, and considering battery degradation allows to trade off arbitrage opportunities with battery lifetime. In the interplay of different types of power and heat generation and storage equipment, there are many degrees of freedom, and hence optimizable decisions. Additionally, we need to consider variations and uncertainty in user behavior (i.e., demand) and prices. We are interested in how different charging strategies for Electric vehicle (EV) batteries, while considering battery degradation, affect overall system cost. In this paper, we analyse the impact of EVs charging strategies on the operational energy costs for a smart neighborhood in an urban setting: a local energy community in Pfreimd, Germany. This community consists of four buildings with 80 apartments combined, connected through a local electricity and a local heat grid. Each building has Photovoltaic (PV) modules installed. Moreover, one building has a small-scale Combined Heat and Power plant (CHP) and a Thermal energy storage (TES). External electricity and district heat grids can provide energy to the local community, while surplus electricity can also be delivered back. We account for battery degradation for both the stationary battery and the EVs, and consider uncertainty in electricity prices and demand. The main contribution of this paper is the combined consideration of vehicle charging strategies, battery degradation, and uncertainty in a smart neighborhood setting.

II. Literature Review

A. Smart Local Energy System

Optimal energy management of smart energy buildings and neighborhoods has recently captured significant attention [4], [5]. Studies focus either on cost-minimization or profit maximization, often via participation in energy markets. Suggested approaches vary according to different perspectives. A first distinction concerns the centralized or decentralized perspective [6], [7]. In a centralized framework, all relevant input data for consumers and prosumers is gathered and assessed via a central entity. In a decentralized framework, this is executed at the local level. Using centralized frameworks leads to lowest costs (or highest profit) [8]. Decentralized structures, however, offer information privacy and other utility to customers in terms of maximized self or local sufficiency by RES.

Despite increasing intermittency and uncertainty for both generation and load, supply has to match demand at all times. Therefore, generation capacity needs to be sufficient to meet maximum demand. Demand Response (DR) can help reduce peak loads and shift loads to periods when generation is high. Through shifting demand, DR can help to handle fluctuating electricity prices and variable supply [9]. Increasing DR efforts enables the accommodation of growing demand, e.g., from EV charging, without expanding the infrastructure [10].

While DR is implemented successfully in the industry, it is lacking in the residential sector. Smart grids in combination with aggregators can enable DR in the residential sector. Aggregators are entities that act as a mediator between individual households and energy utilities. Combining and managing demand and available flexibility from many households allows them to balance energy within their portfolio while handling energy volumes that allow participation in retail and flexibility markets [11].

Dispatchable energy units, e.g., storage's and CHP are especially important in smart grids [12]. The increased flexibility benefits all actors in the system. Furthermore, a TES will allow more efficient operation of the CHP as it decouples the electric and thermal profiles of the CHP, thereby enabling more flexible operation [13]. This, in turn, is very helpful when using the CHP as a balancing source for fluctuating RES (c.f., [14]). Beside (foreseeable) intermittency, uncertainties arising from a variety of sources such as RES, market prices, demand profile, and recently EVs, impact least-cost operation [15]–[18]. Despite a significant impact of uncertainty, most researchers deploy deterministic models (c.f., [6], [19]). Generally, deterministic approaches lead to non-optimal solutions. Accounting for uncertainty gives more robust, lower cost solutions. E.g., [15] use Monte Carlo simulation to investigate how Distributed Generation (DG) units (CHP and power-only units) and EV batteries can be used to mitigate the effects of price uncertainty in Micro Grid (MG) operation.

[20] propose a two-stage stochastic model to optimize the operation of a RES-based MG equipped with an EV parking lot. To account for the risks associated with uncertainties from load, electricity price, EV drivers behavior, PV, and wind generation, they use the conditional value at risk measure. As in energy systems the realization of uncertain events typically happens at multiple moments in time, multi-stage rather than two-stage stochastic programs can be more appropriate. (c.f., [21], [22]). Few papers only develop multi-stage models for operational scheduling in energy systems. [23] compare a two-stage and a multi-stage model for an economic dispatch problem with RES to minimize the expected total cost. They solve a case study based on IEEE 118-bus system using stochastic dual dynamic programming, and illustrate the improvement and robustness of the solution found. [24] apply a multistage stochastic model accomplish more energy-efficient scheduling of a CHP unit, PV, heat boiler, and energy storage systems in a building with electricity and thermal demand. To take advantage of a DR program, load profiles are separated into

a deterministic non-controllable load and a controllable load with a stochastic attribute. They use a rolling scheduling method to reoptimize based on updates of the information on uncertain parameters corresponding to load and PV power generation.

B. Electric vehicles in Smart neighborhoods

EVs have typically up to 90% idle time, which can offer significant flexibility in terms of both (shiftable) demand and (storable) supply (via the battery). The distribution of EV arrival times at home is skewed towards the afternoon. Most EVs connect between 13:00 and 19:00 at work days [25]. Spatiotemporal parameters like charging at home or at work, weekday, the car-type and the charging infrastructure influence the charging schedule, i.e., the load and peaks therein (c.f., [26]).

Managing charging schedules can be beneficial for the operational cost. We can distinguish passive, uncontrolled and active, flexible charging strategies [27]. Uncontrolled, *passive charging* means that vehicles charge, from the moment they are plugged in, at the maximum possible charge power until the battery is full. Flexible approaches may be *controlled*, when an aggregator controls EV charging schedules directly, or *incentivised*, when she provides price signals to incentivize users to charge at moments most convenient for the broader system. A flexible approach only managing the charging schedule is *smart charging*, while a charging schedule that also allows discharges is Vehicle-to-Grid (V2G). Naturally, V2G provides the most flexible charging scheme, but may create additional stress on the EV battery [27], leading to degradation, and reduced battery lifetime. While many studies have investigated the interplay between EVs and smart neighborhoods, they ignore degradation costs when evaluating charging strategies [15], [18].

C. Battery degradation

Battery lifetime has two components, calendar and cycle life, that both reduce through chemical and mechanical stress [28]. In frequently used batteries, cycle life tends to be the decisive lifetime component [29]. This is the case in stationary batteries, while for EV batteries, with up to 90% idle time, calendar aging tends to be the dominant influence. As the two aging behaviors are additive, both should be minimized [30], [31].

Avoiding battery degradation can be done by accounting for penalties per kWh throughput and State of Charge (SOC) boundaries [32], [33]. However, such simple representations disregard the quadratic increase of Cycle Depth (CD) based aging and ignore other aging mechanisms. Typically, this results in relatively deep cycles and high resting SOC levels, causing the actual battery degradation to be (potentially much) larger than the model shows. To better account for nonlinear or even non-convex characterizations of degradation, researchers have used advanced optimization methods, such as Mixed-Integer-Linear-Programming (MILP) [34]–[36], and mixed-integer Non-Linear-Programming (NLP) [37]. MILP methods are able to model on/off decisions for equipment and incorporate piecewise linear functions, thereby providing good approximations of nonlinearities – often with lower computational complexity compared to NLP. They are well-suited for energy management problems in the context of smart neighborhoods. Specifically for approximating CD based degradation, piecewise linear functions using segments is commonly used [38]–[40]. Concerning V2G strategies there is mixed evidence for their viability as the additional degradation costs can be prohibitive (c.f., [41] where high charge powers cause significant damage to the battery). As we also see in our case study, in other cases the arbitrage benefits outweigh the increased degradation costs. More complex degradation models, like an open circuit model, however, often become non-convex [42].

In [43] we propose and test a scalable, MILP battery degradation model considering three degradation components, which we integrate in this paper in a stochastic multi-stage optimization model for a smart neighborhood. For the cycle aging, we consider a segmented CD model, in which cycles are penalized more than proportional with CD [43]. The penalty is calculated according to Eq. (1) [44].

$$Q^{CD}(CD) = A \cdot CD^{\frac{1}{m}} \tag{1}$$

Additionally, we consider the average SOC within a cycle, represented by binary constraints. The penalty increases symmetrically with the SOC's distance to 50% SOC [43]. The third mechanism is SOC-related calendar aging [31], [43]. We ignore charge-rate dependent degradation as stationary batteries with low power to energy ratios can not reach damaging charge rate levels over 1C. Additionally, moderate charge rates imply a low temperature gradient in the battery [41]. Further, the ambient temperature impact is hard to model, as it sets the cell temperature's initial level but can deviate significantly from it, especially for actively used batteries in low ambient temperature conditions.

III. Model Formulation

We present the model in its general form, allowing V2G.

A. Objective function

$$\begin{aligned} MIN: \sum_{h} \alpha_h \cdot \Bigg[& \sum_{b,e} (p_{e,h} \cdot G_{b,e,M,h} \\ & - v_{e,M} \cdot (p^{RES} \cdot I^{RES}_{b,e,M,h} + p^{CHP} \cdot I^{CHP}_{b,e,M,h})) \\ & + \sum_{b} (p_{gs,h} \cdot CHP^{in}_{b,h} + k^{O} \cdot CHP^{out}_{b,el,h}) + \sum_{b,w} K_{b,w,h} \Bigg] \\ & + \sum_{b,w,\hat{h}} (\alpha_h \cdot (SOC_{b,w,el,0} - SOC_{b,w,el,\hat{h}}) \cdot k^{end}) \end{aligned} \tag{2}$$

The model minimizes expected operational energy costs Eq. (2). The first term describes the energy purchased from the main grid, and the second term the feed-in remuneration from injecting into the main grid. Here, the feed-in is separated into RES and CHP as they may have different selling prices.

The next terms, on the third line are the CHP gas input costs and operational costs per kWh_{el} produced. The last term on the third line is the battery degradation costs K. On the fourth line we include a penalty (a bonus for negative values) for the deviation of SOC levels at the end of the planning horizon and the starting SOC. For the smart and V2G charging schemes, we penalize the delta of the starting SOC and the SOC at the end of the optimization horizon. Thereby, we account for the need to have EVs fully charged at their departure, but allow lower SOC values in some scenarios if alternative electricity supply would be very expensive.

B. Constraints

We omit the scope of some constraints to allow fitting them on a single line. E.g., in Eq. (3) the scope is $\forall\ b, e, h$.

1) Grid constraints: Eq. (3) is the energy balance. For every building, hour, for both electricity and gas, the supply in form of RES and CHP generation, grid import, stationary and vehicle storage discharges equals the sum of residential demand, potential curtailment, grid exports, and storage demand. We allow curtailment because heat cannot be delivered to the main grid, and this might unnecessarily prevent the CHP from generating electricity. Here, only main grid injections are efficiency adjusted. We apply the local grid efficiency in Eq. (4), the balance for local generation and injections correctly. All round-trip efficiency losses are accounted when injecting.

$$\sum_{t} g^{RES}_{b,t,e,h} + CHP^{out}_{b,e,h} + \sum_{n} G_{b,e,n,h} + \sum_{w,j} D_{b,w,e,j,h} = dem_{b,e,h} + CU_{b,e,h} + \frac{I_{b,e,M,h}}{v_{e,M}} + I_{b,e,L,h} + \sum_{w,j} C_{b,w,e,j,h} \tag{3}$$

$$\sum_{b} G_{b,e,L,h} = v_{e,L} \cdot \sum_{b} I_{b,e,L,h} \qquad \forall\ e, h \tag{4}$$

We do not allow heat injection into the main grid and set $I_{b,ht,M,h} = 0, \forall b, h$. Thus excess heat is either stored in the TES or curtailed. The upper bound for RES-based grid injections is the RES production Eq. (5) .

$$I^{RES}_{b,e,M,h} \leq v_{e,M} \cdot \sum_{t} g^{RES}_{b,t,e,h} \qquad \forall\ b, e, h \tag{5}$$

2) Storage constraints: The storage level at the start of a time step equals the storage level of the previous time step adjusted for, loss-corrected, charges or discharges (Eq. (6)). To enable the consideration of CD based degradation, we divide batteries into virtual segments J with equal sizes and segment specific costs. Eq. (7) imposes segment-level storage limits. Eqs. (8) and (9) restrict charges and discharges to their maximum values. We assign a parameter value $S_{b,w,e,j,h^{arr}} = S^{arrival}_{b,w,e,j,h}$ to arriving EVs. In following time steps, for connected EVs, Eq. (6) applies. For the departure time step, we impose $S_{b,w,el,j,h^{dep}} = e^{rated}_{b,w,el}$ to assure a fully charged EV.

$$S_{b,w,e,j,h} = S_{b,w,e,j,\tilde{h}} + v^{c}_{b,w,e} \cdot C_{b,w,e,j,\tilde{h}} - \frac{D_{b,w,e,j,\tilde{h}}}{v^{d}_{b,w,e}} \tag{6}$$

$$S_{b,w,e,j,h} \leq \frac{e^{rated}_{b,w,e}}{|J|} \tag{7}$$

EV batteries are modelled as stationary batteries, with the addition of arrival and departure times [45]. Thereby EVs act as a (dependent on the charging strategy, possibly flexible) demand and as storages in given time periods. The presence of EVs is reflected by parameter $a_{b,w,h} = 1$. Consequently, $a_{b,w,h} = 0$ imposes zero as upper limits in Eqs. (8) and (9). For stationary storages, all $a_{b,w,h} = 1$.

To model degradation, details in the next Section, binary variables indicate three mutually exclusive states Eq. (11): charging, discharging and steady state. (Eqs. (8) to (10)).

$$\sum_{j} C_{b,w,e,j,h} \leq c^{max}_{b,w,e} \cdot a_{b,w,h} \cdot B^{C}_{b,w,e,h} \ \forall\ b, w, e, h \tag{8}$$

$$\sum_{j} D_{b,w,e,j,h} \leq d^{max}_{b,w,e} \cdot a_{b,w,h} \cdot B^{D}_{b,w,e,h} \ \forall\ b, w, e, h \tag{9}$$

$$1 - \sum_{j} (D_{b,w,e,j,h} + C_{b,w,e,j,h}) \leq B^{S}_{b,w,e,h} \ \forall\ b, w, e, h \tag{10}$$

$$B^{C}_{b,w,e,h} + B^{D}_{b,w,e,h} + B^{S}_{b,w,e,h} = 1 \qquad \forall\ b, w, e, h \tag{11}$$

A *passive charging* mode can be represented by imposing adequate minimum SOCs levels for the relevant time steps. For *smart charging*, we only impose a full battery at the departure time, and do not allow discharges.

C. Battery degradation

We use the battery degradation constraints developed in [43]. The degradation cost K (Eq. (12)) has three components $Q^{CD}_{b,w,el,h}$ - the cycle depth degradation, $Q^{SOC}_{b,w,el,h}$ - the average SOC cycle degradation, and $Q^{CAL}_{b,w,el,h}$ - the calendar degradation. The component wise % capacity losses are multiplied by the battery replacement cost (€/kWh) and battery capacity (kWh).

$$K_{b,w,el,h} = R \cdot e^{rated}_{b,w,el} \cdot (Q^{CD}_{b,w,el,h} + Q^{SOC}_{b,w,el,h} + Q^{CAL}_{b,w,el,h}) \quad \forall\ h \tag{12}$$

1) Cycle Depth degradation: Eq. (13) determines the CD based damage considering J segments, which is accounted for during discharging. Discharges in consecutive time steps are part of the same cycle, which needs to be handled. The first term in Eq. (13) locates how much of which segments is discharged in the current time step, while the second term provides the degradation value.

$$Q^{CD}_{b,w,el,h} = \sum_{j} \left(\frac{D_{b,w,el,j,h}}{\frac{e^{rated}_{b,w,el}}{|J|}} \left[Q^{CD}\left(\frac{j}{|J|}\right) - Q^{CD}\left(\frac{j-1}{|J|}\right) \right] \right) \tag{13}$$

2) Average cycle SOC degradation: Quite some bookkeeping is needed to account for this type of degradation. We compute several auxiliary values, which are used to apply a

penalty at the end of a discharge cycle only. Eq. (14) computes the relative SOC at the end of every hour.

$$SOC_{b,w,e,h} = \frac{\sum_j S_{b,w,e,j,h}}{e^{rated}_{b,w,e}} \qquad \forall\ b,w,e,h \quad (14)$$

Following [43], Eqs. (15) to (17) and Eqs. (18) to (20), use the binary variables to determine start respectively end points of specific discharging half cycles. Eq. (15) only allows the start of a discharging cycle, if for h the battery is discharging, but in previous time step $\tilde{h}$ it was not. Eq. (16) only allows the start of a discharging cycle, if for h it is discharging. Eq. (17) disallows the start of a discharging cycle, if for $\tilde{h}$ the battery was discharging already. These three combined appropriately determine the start of discharging cycles.

$$B^{St}_{b,w,el,h} \geq B^{D}_{b,w,el,h} - B^{D}_{b,w,el,\tilde{h}} \qquad \forall\ b,w,h \quad (15)$$
$$B^{St}_{b,w,el,h} \leq B^{D}_{b,w,el,h} \qquad \forall\ b,w,h \quad (16)$$
$$B^{St}_{b,w,el,h} \leq 1 - B^{D}_{b,w,el,\tilde{h}} \qquad \forall\ b,w,h \quad (17)$$
$$B^{END}_{b,w,el,h} \geq B^{D}_{b,w,el,\tilde{h}} - B^{D}_{b,w,el,h} \qquad \forall\ b,w,h \quad (18)$$
$$B^{END}_{b,w,el,h} \leq B^{D}_{b,w,el,\tilde{h}} \qquad \forall\ b,w,h \quad (19)$$
$$B^{END}_{b,w,el,h} \leq 1 - B^{D}_{b,w,el,h} \qquad \forall\ b,w,h \quad (20)$$

In Eq. (21), the first term saves the SOC at the start of a discharge cycle in auxiliary variable A^{St}. In following time steps, the second term keeps this value in the cache. After the cycle end, the auxiliary must be reset before the next cycle. Hence, the second term checks if a cycle ended in the previous scenario node, to set the variable back to zero.

$$A^{St}_{b,w,el,h} = SOC_{b,w,el,h} \cdot B^{St}_{b,w,el,h} + (1 - B^{St}_{b,w,el,h} - B^{END}_{b,w,el,\tilde{h}}) \cdot A^{St}_{b,w,el,\tilde{h}} \qquad \forall\ b,w,h \quad (21)$$

This starting SOC is then passed to Eqs. (22) and (23) that compute the deviation of the average SOC to 50%.

$$A^{cyc}_{b,w,el,h} \geq \frac{SOC_{b,w,el,h} + A^{St}_{b,w,el,h}}{2} - \frac{1}{2} \qquad \forall\ b,w,h \quad (22)$$
$$A^{cyc}_{b,w,el,h} \geq \frac{1}{2} - \frac{SOC_{b,w,el,h} + A^{St}_{b,w,el,h}}{2} \qquad \forall\ b,w,h \quad (23)$$

Finally, in Eq. (24) we penalize the absolute deviation A^{cyc} with the penalty factor f. However, this penalty is only active at the end of each cycle. Thus we penalize the average deviation over the cycle once and not every period.

$$Q^{SOC}_{b,w,el,h} = f \cdot A^{cyc}_{b,w,el,h} \cdot B^{END}_{b,w,el,h} \qquad \forall\ b,w,h \quad (24)$$

3) Calendar degradation: For the calendar life loss Q^{CAL} we use a piecewise linearization using SOS2 variables that define which line segment of the linearization is active. Eq. (25) computes the SOS2 weighting factor $Z_{b,w,el,i,h}$. Eq. (26) computes the calendar aging. Eq. (27) ensures that the interpolation weights sum up to 1. Eq. (28) ensures only one segment can be active. Eq. (29) ensures that interpolation weights can only be positive for the active line segment.

$$SOC_{b,w,el,h} = \sum_i (o^{CAL}_{b,w,i} \cdot Z_{b,w,el,i,h}) \qquad \forall\ b,w,h \quad (25)$$
$$Q^{CAL}_{b,w,el,h} = \sum_i (y_{b,w,i} \cdot Z_{b,w,el,i,h}) \qquad \forall\ b,w,h \quad (26)$$
$$\sum_i Z_{b,w,el,i,h} = 1 \qquad \forall\ b,w,h \quad (27)$$
$$B^{CAL}_{b,w,el,i,h} + B^{CAL}_{b,w,el,m,h} \leq 1 \qquad \forall\ b,w,i,m > i+1,h \quad (28)$$
$$Z_{b,w,el,i,h} \leq B^{CAL}_{b,w,el,i,h} \qquad \forall\ b,w,i,h \quad (29)$$

D. CHP Operation

We model CHP operation with a piecewise segmentation. Eq. (30) and Eq. (31) define the energy input and output.

$$CHP^{in}_{b,h} = \sum_u o^{CHP}_{u,gs} \cdot X_{u,h} \qquad \forall\ b,h \quad (30)$$
$$CHP^{out}_{b,el,h} = \sum_u o^{CHP}_{u,el} \cdot X_{u,h} \qquad \forall\ b,h \quad (31)$$

The CHP has several breakpoints, including an *off* state and a minimum operating level. Eq. (32) ensurs that the first breakpoint can only be active alone, enforcing zero input and output. For the remaining breakpoints Eq. (33) enforces that only one line segment can be active at the same time. Eq. (34) ensures that the sum of the weights $X_{u,h}$ equals 1. Finally, Eq. (35) guarantees that weights can only be positive for active segments.

$$B^{CHP}_{1,h} + B^{CHP}_{u,h} \leq 1 \qquad \forall\ u > 1,h \quad (32)$$
$$B^{CHP}_{u,h} + B^{CHP}_{u+2,h} \leq 1 \qquad \forall\ u,h \quad (33)$$
$$\sum_u X_{u,h} = 1 \qquad \forall\ h \quad (34)$$
$$X_{u,h} \leq B^{CHP}_{u,h} \qquad \forall\ u,h \quad (35)$$

IV. Case Study

We start with analyzing a set of deterministic cases to provide a clear understanding of what is driving the operational dynamics of the system when considering the three different charging schemes while accounting for battery degradation. Next, we consider the influence of uncertainty in both main grid electricity prices and the SOC of EVs when they arrive at the building complex in the late afternoon. All cases are solved using Pyomo with Gurobi version 9.1.2 [46]. The model runs on a Lenovo ThinkSystem SD530 with CPU@ 2x 3.5GHz Intel Xeon Gold 6144 CPU – 8 core and 384GB RAM. With this setup, the deterministic V2G case solves in 86.61 seconds. Due to increased complexity in the stochastic case, we set the gap tolerance to 0.1% which results in a solve time of 19 minutes and 12 seconds.

A. Input data

The building complex data are based on an existing complex in Pfreimd, Germany. It consists of three high-rise and one lower apartment building with in total 80 apartments and about 300 residents. All buildings have rooftop PV modules, and there are local grids for heat and electricity. Moreover, the buildings are connected to the main grids for electricity and district heating. One of the buildings features a small-scale

CHP, and a TES. To reflect a potential future situation of interest, we add a stationary electric battery to the complex, and add EV charge stations on the parking lot. We consider

TABLE II: CHP characteristics [47]

Operating Level [%]	0	50.0	75.0	100.0
Gas consumption [kW]	0	37.1	48.1	61.1
Electric output [kW]	0	10.0	15.0	20.0
Heat output [kW]	0	28.1	34.2	42.2

an hourly time resolution. For the specific day considered, Monday the third of June 2019, the complex had a residential peak electricity demand of 68 kW and a peak heat demand of 43 kW. The PV modules peak generation at this date was 73 kW. This was larger than peak demand, which will induce battery charging and / or grid exports in the model. Table II presents the CHP output and efficiency for four different operation modes. The model determines the operational level using interpolation, as explained above in Section III-D. The maximum CHP heat output is just short of covering the peak demand, so some heat supply must come from the main grid or the TES. Table III summarizes the storage data. In the case

TABLE III: Storage data

Storage type	Battery	TES	EV (each)
Capacity [kWh]	150.0	172.0	40.0
Power [kW]	90	42.2	7.0
Round trip efficiency [%]	90.0	90.0	88.0
Assumed operating temperature [°C]	25.0	–	25.0
A in Eq. (1) [%/cycle]	0.04519	–	0.04519
m in Eq. (1)	0.4926	–	0.4926
f [%/cycle]	0.0085	–	0.0085

set up, we include six EVs with the battery dimensions of a typical Nissan Leaf [48]. For the replacement cost R, we assume 150 €/kWh [49]. The round trip efficiency of the EVs is assumed to be slightly lower than for the stationary battery. We base the cycle degradation parameters A, m, f on measurements from [44]. For the calendar degradation we use measurements from [31] but divide them by 4 as various studies show significantly lower degradation values [50]–[52]. Hence, the battery can experience up to 2% capacity loss per year (equal to ten-year shelf life). All degradation data is valid for a nickel manganese cobalt battery chemistry.

TABLE IV: Calendar aging values at segment breakpoints in $10^{-4}\%$

o^{CAL}	0%	30%	60%	70%	100%
y	1.50	3.50	4.0	7.43	8.93

The hourly electricity prices are based on the German spot prices for this specific date; we add the network fee (7.39 ct/kWh [53]) and value-added tax (19%). For the gas price, we assume a constant $6.145\ ct/kWh$, the average gas price for German household consumers in 2019, including network charges and tax [54]. In addition to the gas costs, the CHP has operational costs of $1.7\ ct/kWh_{el}$, based on the service contract of the building complex. We assume a constant $8\ ct/kWh$ as the district heating grid price. In line with regulations for feed-in tariffs concerning PV modules with peak power $\leq$ 100kW, the excess PV power can be sold at a fixed rate of 6.59 ct/kWh [55]. This encourages self consumption, possibly via own storage.

For the EV availability parameter $a_{b,w,h}$, we use the distribution from [25] for week days. We consider three car groups with two cars each, with arrival times: 16:00, 17:00, and 20:00, with respective SOC levels of 50%, 60%, and 40%.

Finally, we need to address the treatment of the arrival SOC and the virtual battery segmentation of EVs in the model. An EV battery always arrives at the neighborhood with the *expensive* segments filled. E.g., an EV that arrives with 50% SOC, arrives with the bottom 10 out of 20 segments filled. Thereby, we account for the discharge while driving. If we would not specify this, the model would fill the cheap battery segments, which represent less battery degradation. In the V2G case, upon arrival, this would lead to very cheap EV discharges and thus a misrepresentation of the degradation in an V2G charging scheme. All in all, the EV was already discharging and thus experiencing degradation while driving which must be acknowledged by the model.

B. Deterministic Case

We consider three EV charging strategies: *passive*, *smart*, and V2G.

1) Passive charging: Fig. 1a displays generation, battery discharges, and grid imports as positive values, while demand, battery charges, and grid exports are negative values. At the start of the day, from 00:00 to 03:00, the CHP runs at full capacity, at a slightly lower level until 05:00 (when solar generation is starting), and at a more reduced load until 09:00. As such, CHP covers most of the electric and the entire heat demand during the night, while also charging the TES.

In the morning after 9:00 PV generation continues to rise, and the CHP shuts down until the evening. Surplus PV power not immediately needed to cover demand, is used for two purposes. First, some of it is sold to the main grid. Here we note that the specific selling hour does not affect the timing of sales, due to the fixed feed-in remuneration.[1] Second, stationary and EV batteries are charged. The rather low feed-in tariff means that the opportunity cost of PV generated electricity is only 6.59 ct/kWh, which is lower than the lowest hourly price when buying from the grid. The stationary battery charges gradually over the day with a big charge to the max SOC right before the first EVs arrives. Again, due to fixed feed-in remuneration, there is no price arbitrage opportunity concerning the timing of selling the grid or charging the battery. In fact, the charging schedule is optimized to minimize the calendar aging of the battery by keeping the battery at a low SOC during most of the day.

Fig. 1c shows the SOC profiles of all battery groups. For EVs an SOC of zero indicates that they are not present at the charger. By assumption, the start and end SOC levels of the stationary battery are 30%. The EVs start at time 00:00 with

[1]Generation costs from the CHP are too high to profitably sell to the grid at any time.

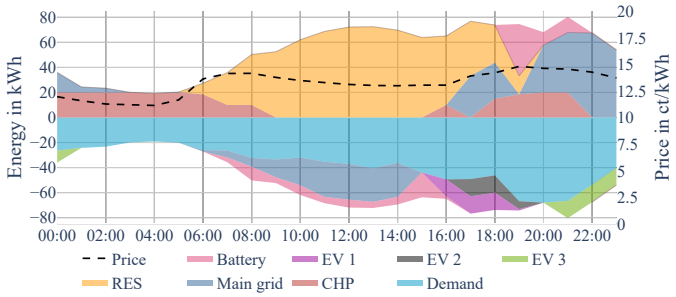

(a) Hourly mass balance electricity–*passive* charging, Deterministic

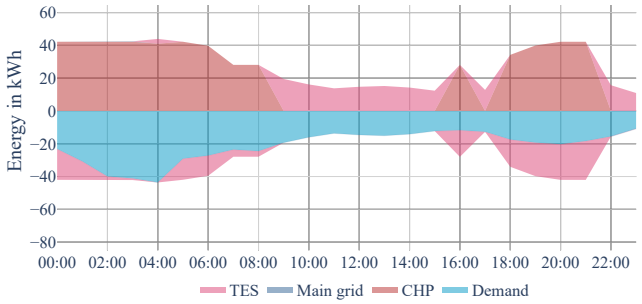

(b) Hourly mass balance heat–*passive* charging, Deterministic

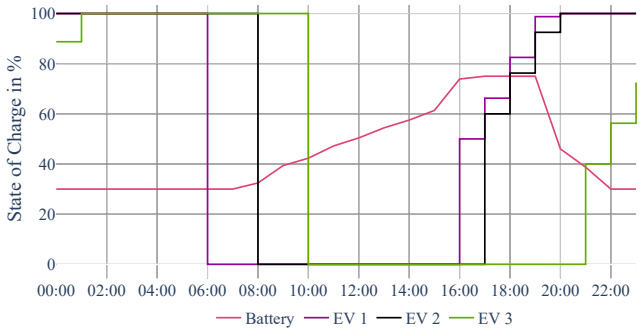

(c) Battery and EV SOC profiles - *passive* charging, Deterministic

Fig. 1: *Passive* charging, Deterministic

SOC levels equal to the last time step: EV1 and EV2 start the day at 100%, and EV3 at 90%. The latter charges one hour at the beginning of the day to reach 100%.

During the entire evening, there is a high residential and EV demand. As soon as an EV connects, it starts charging at maximum capacity. Additionally, the PV generation declines rapidly after 18:00, leading to a spike in grid imports around 20:00, when electricity prices are at their highest for the day. Therefore, the stationary battery discharges during these hours to avoid main grid import costs.

As a side note, the TES, which is preset to start with exactly and end the day with at least 30% of capacity, is charged by the CHP to 64%. It can thereby cover the heat demand between 09:00 and 15:00. Consequently, the neighborhood is self-sufficient for heat this summer day.

The EV charge load is more than 12% of total electricity demand. Adding this load to the residential demand increases the total energy costs by almost 30% (from 66.86€ to 86.45€). *Passive charging* imposes that EVs are mostly charged when electricity prices are highest.

2) Smart charging: Here, we allow the model to determine when to charge the EVs, given the same starting SOC levels as above, and impose a full charge upon departure.

Fig. 2 shows a significant change in the charging schedule compared to the passive charging. The EVs start the day with their low arrival SOC from the night before. Thus, they charge during the lowest price period. In terms of DR, we see valley filling: EV demand shifts towards the low residential demand, low-price period between 02:00 and 05:00. This flexibility has two benefits. First, the EVs charge at the lowest possible energy cost. Second, they avoid calendar aging as the SOC stays low until shortly before departure. In Table V, we see that the annualized battery degradation is reduced by 29%. As we apply cycle aging only during discharge periods and discharges are not allowed, this reduction is entirely due to reduced calendar aging due to delayed charging.

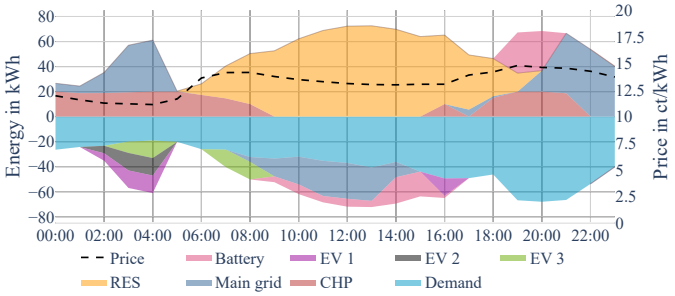

(a) Hourly mass balance electricity – *smart* charging, Deterministic

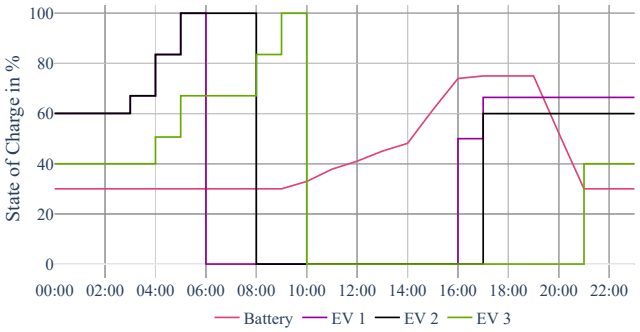

(b) Battery and EV SOC profiles – *smart* charging, Deterministic

Fig. 2: Smart charging – Deterministic

Smart charging reduces main grid imports by 4%, and peak imports by as much as 20%. Total grid exports are reduced by 15%. Compared to passive charging, EV1 charges 5 kWh extra in the evening. This leads to a higher SOC at 23:00 than at 0:00. This is driven by the SOC deviation penalty acting as a reward, as its value is higher than the sales value of surplus PV. This reflects the value of a lower charging load the following day. For EV1-2 there is not enough time left the next morning to charge fully to benefit from lower prices. This all points to higher self-consumption of PV power.

The overall cost increase due to EV charging is almost 20% (from 66.86€ to 80.16€), one third lower than the 30% in

TABLE V: Deterministic Case KPI

KPI	Passive	Smart	V2G
Objective value [€]	86.45	80.16	80.13
Battery throughput [kWh]	64.12	64.12	64.12
PV generation [kWh]	681.13	681.13	681.13
Electric CHP generation [kWh]	241.31	242.50	242.50
Peak demand [kW]	80.46	68.08	68.08
Peak grid import [kW]	67.64	53.81	53.81
Total grid import [kWh]	294.01	273.42	268.82
Total grid export [kWh]	161.08	136.34	136.34
Annualized stationary battery aging [%]	4.12	4.11	4.11
Average annualized EV battery aging [%]ˆ	1.17	0.83	1.02

ˆWe neglect degradation from discharges while driving; the model only accounts for EV battery degradation while connected to the charger.

passive charging. Part of this cost saving is caused by 29% lower EV battery degradation. We can conclude that more flexible charging is beneficial for the whole neighborhood by reducing the peak load, grid dependency, and cost, as well as the individual EV owner by prolonging the EV life.

3) V2G charging: Here, we allow the model to let EVs discharge. We set the minimum SOC at 0:00 to 30% for all batteries. Overall, the hourly electricity balance is very similar in Fig. 3a in comparison to Fig. 2a. The charging hours are the same. The major difference is in the evening. EV1 discharges from 19:00 to 21:00. Thereby, it reduces the grid imports during the highest prices of the day and in total by 1.68 % (Table V). Despite slightly higher round-trip losses of the EV compared to the stationary battery, the former is preferred over the latter. The stationary battery does not exceed 75% SOC.

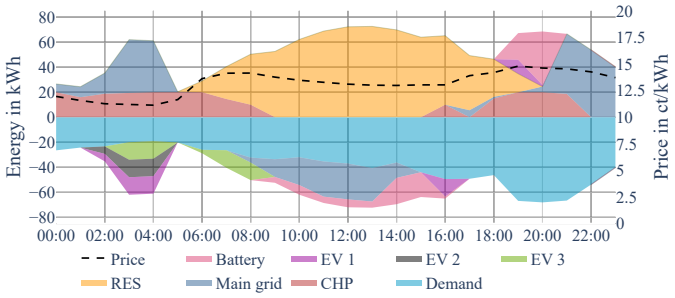

(a) Hourly mass balance electricity–*V2G* charging, Deterministic

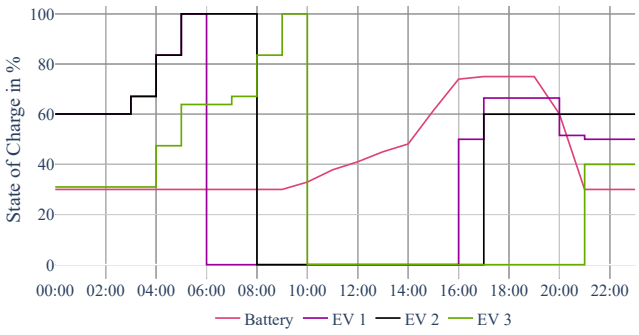

(b) Battery and EV SOC profiles – *V2G* charging, Deterministic

Fig. 3: V2G - Deterministic

This is because the SOC profile is less damaging, as its average stays close to 50%. Here, V2G allows a more optimal usage of the stationary battery as degradation costs of all batteries are traded off optimal against all other decisions. Additionally, to benefit from the deviation reward, the optimal EV3 SOC at 0:00 is 30%, implying a 10% discharge in the last hour of the previous day. Only EV3 can benefit, as it has a late enough departure time to allow cheap charging directly from PV between 06:00 and 09:00 in the morning.

Compared to smart charging, the reduction in total system costs is very small, while EV battery degradation increases by 23% due to the discharges. A slightly higher value for battery replacement costs might have resulted in no discharges at all.

C. Stochastic Case

The effects of two sources of uncertainty are explored: the arrival SOC and the electricity price. We consider three moments during the day where uncertainty is revealed. At each price branching point, the medium scenario has a probability of 40% and low and high scenarios both consider 30% probability for deviations of 10% down and up respectively. Price branches occur at 05:00 and 20:00, which we have chosen based on battery activity and price levels in the deterministic cases. Price uncertainty during the day would not have much impact, as the surplus PV generation is sold at a fixed feed-in tariff. The price deviations are additive, resulting in five different price levels after 20:00 (c.f., Fig. 4).

EV1 and EV2 have expected arrival SOC levels of 50% and 60% respectively, that occur with a probability of 80%. Additionally, with 10% probability, EVs1-2 can arrive with 10% total battery capacity, i.e., 16 kWh higher or lower combined SOC level. Furthermore, although EV2 arrives one hour later, the branching on the arrival SOC happens at 16:00. We ignore SOC uncertainty for EV3 as we have seen that its late departure time in the morning allows charging using cheap power, and to reduce the number of scenarios and ensure model tractability. Additionally, we deactivate Q^{SOC} (Eq. (15)-Eq. (24)), as it significantly increases the model solution time, but is the degradation mechanism with the least impact on the overall degradation. To distinguish the

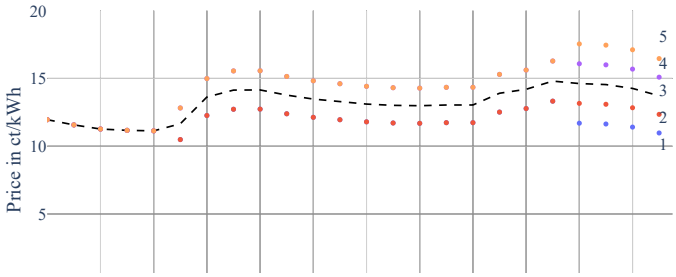

Fig. 4: Stochastic price scenarios

27 scenarios, we construct identification codes *PXN*. The first letter represents the first price branch, while the second letter represents the arrival SOC branch: low (L), medium (M), and high (H). The number for the second price branch is explained by Fig. 4. Thus, LL1 is the scenario: low first price, low arrival SOC, low second price.

Please be aware that in many Figures the axes have been truncated for readability. We illustrate system behavior by contrasting selected results of five of the 27 scenarios.

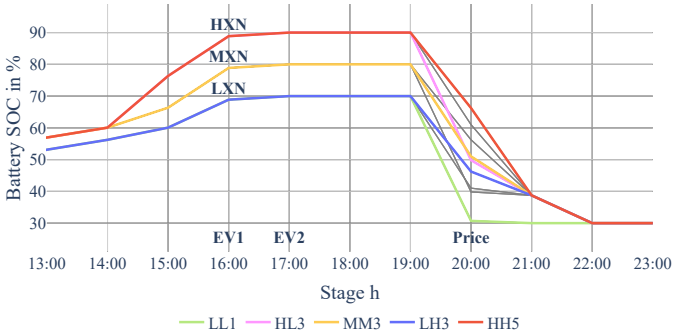

Fig. 5: Stationary battery SOC profiles – *V2G* charging, Stochastic.

1) Stochastic - Passive charging: The EVs charge at maximum power as soon as they arrive. Consequently, different charging pattern are only due to different arrival SOC. However, Fig. 5 shows that the stationary battery discharge paths do vary according to the scenario path. Firstly, the first price branch at 05:00 leads to three SOC paths. In all *LXN* scenarios the stationary battery reaches a maximum SOC of 70%, in all *MXN* scenarios 80%, and in all *HXN* scenarios 90%. To illustrate the effect of uncertainty, consider the middle ground *expected value* scenario *MM3*. Compared to the deterministic case, the battery charges 5% more under the same conditions, due to taking uncertainty into account.

We see battery discharges starting at 19:00, the hour with the highest price in the deterministic setting. Comparing *LL1* and *LH3* shows the impact of arrival SOCs. In *LH3*, EV1 arrives at 16:00 with a high SOC and is fully charged by 19:00. Therefore, the stationary battery can wait with discharging until after the last price split occurs. In the high price scenarios *HX5*, the highest price in the day occurs at 20:00 and not 19:00. This is however not known until it is 20:00. Therefore, the largest discharge in all scenarios happens at 19:00 and the second price uncertainty does not affect the battery discharge scheduling in a passive charge scheme.

2) Stochastic - Smart charging: Fig. 6 shows the same three maximum stationary battery SOC levels as for passive charging. EV2-3, charge in the morning, while EV1 utilizes the same amount of PV power upon arrival in all scenarios (Fig. 7). In the later evening only the residential demand has to be met, partly covered from the stationary battery, which has no discernible variation in the discharge pattern in the three branches. Thus, with smart charging, the arrival SOC and the second price split do not affect the stationary or EV behavior.

3) Stochastic - Vehicle to Grid: Fig. 8 shows a similar V2G stationary battery profile as for smart charging. However, EV discharges do lead to slight changes in the stationary battery.

For instance, *LH3* and *HH5* both have high arrival SOCs. In the low price scenario EV discharge happens only after the price branch at 20:00, while in *HH5* EV1 already discharges at 19:00. This has two reasons. First, EVs have to be fully charged by their departure, while the stationary battery has

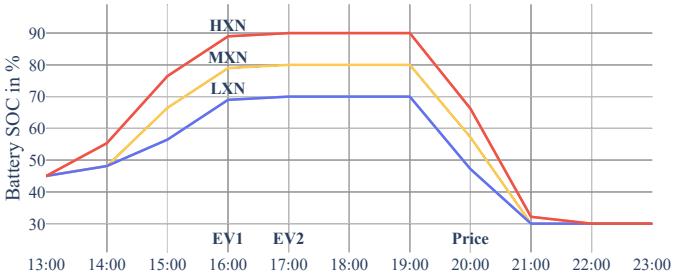

Fig. 6: Stationary battery, Smart charging, Stochastic

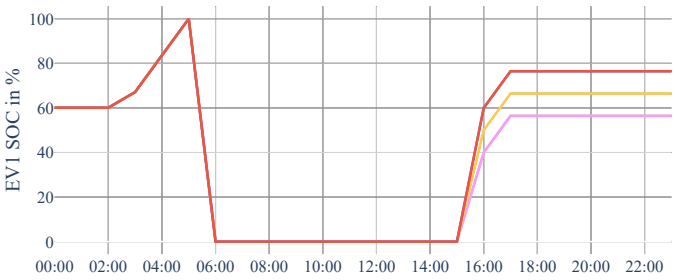

Fig. 7: EV1, Smart charging, Stochastic

a minimum SOC of 30% at midnight. Therefore, the EV discharge awaits the last price realization. Is it high, then the EV starts discharging, is it low, it doesn't (c.f., the two grey *LH1* and *LH2* branches above *LH3* in Fig. 9) The consistently high prices in *HH5* lead to an EV1 discharge at 19:00 because the initial high price split at 5:00 makes it beneficial in all following scenarios *HXN*. In these scenarios, the stationary battery discharges less at 19:00, the EV more. Thereby, the EV SOC drops from 76% to 60%, which leads to a significant reduction in calendar aging. *LH3* and *HL3* show similar behavior. The EV only discharges after 20:00 if that is beneficial. The difference in *HL3* is the higher maximum SOC of the stationary battery, while the EV arrives with a lower SOC. However, we see the same discharge scheduling of both the stationary battery and the EV in both cases, which shows that the EV discharge decision is rather independent of the stationary battery.

In *HH5* EV2 also discharges to avoid high price grid imports, while in *LL1* there are no EV discharges at all. We can conclude that, the particular benefit of the V2G discharging is

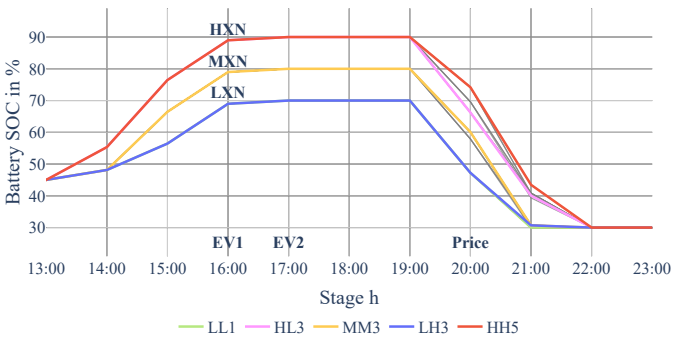

Fig. 8: Stationary battery, V2G charging, Stochastic

in the scenarios ending in high prices.

Overall, we see only few occurrences of EV discharges. There are several conditions that must both allow it and make it optimal. First, EV1 arrives early and can charge one hour with cheap PV power. This increases the opportunity for price arbitrage. Second, it has to be more beneficial than other alternatives. PV, CHP and the stationary battery are cheaper alternatives in most situations. Furthermore, V2G charges and discharges can only happen when the EV is connected, and price arbitrage is possible during this time. Finally, the charge and discharge power must be high enough to accommodate charges and discharges on top of reaching a full charge. Higher power ratings allow for more flexible schedules, because low price situations can be exploited more aggressively, but may aggravate degradation. All in all beneficial V2G usage has five criteria:

1) Electricity price volatility
2) Alternative energy sources
3) Period of availability
4) The difference between arrival and departure SOC
5) Maximum charge and discharge power

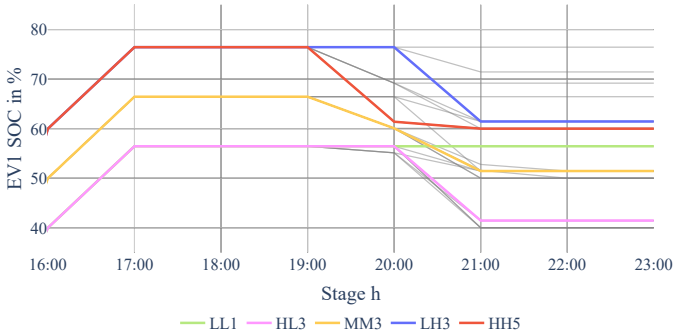

Fig. 9: EV1, V2G charging, Stochastic

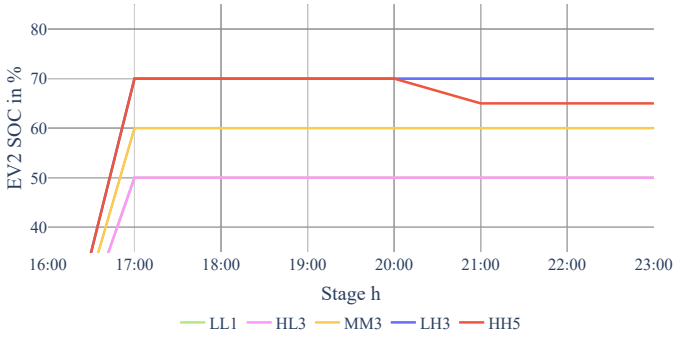

Fig. 10: EV2, V2G charging, Stochastic

Fig. 11 presents the system cost for the three charging schemes. CHP costs are the same and make up more than half in all five scenarios shown, as it only covers demand and never sells to the grid. By contrast, net grid exchange costs vary significantly. Net grid import costs gradually increase from *LL1* to *HH5*. Especially in scenarios *HXN*, battery degradation costs are higher due to higher battery discharges, which mitigate some of the high price consequences. Of these five scenarios, *HL3* and *HH5* see the highest battery degradation costs at 5% of total costs, which is substantial. Furthermore, given relatively modest price variations over the day, the stationary battery does cycle only once. This causes its degradation to not depend on the EV charging scheme but rather on the initial price path that determines its maximum SOC level during the day.

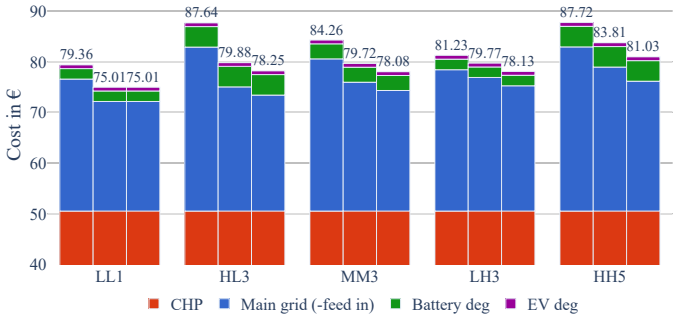

Fig. 11: Decomposed costs, left: Passive, middle: Smart, right: V2G

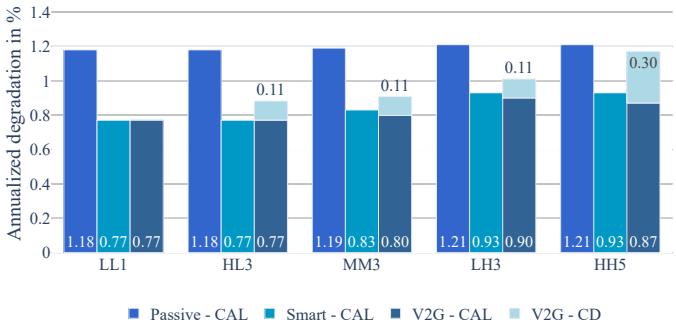

Fig. 12: EV degradation, left: Passive, middle: Smart, right: V2G

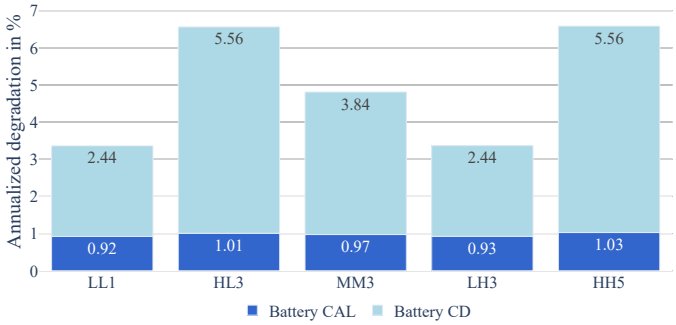

Fig. 13: Battery degradation, differences in charging schemes are less than 0.01%, thus we only show the result of one scheme

The EV degradation is only a small part of the overall system costs. Fig. 12 shows that the EV degradation (while connected) ranges from 0.77 to 1.21%. For all charging schemes, calendar degradation is the primary EV degradation factor. This is different from the stationary battery, for which CD degradation is the biggest contributor (Fig. 13). Overall,

the benefit of V2G increases with larger uncertainty. In the middle ground scenario *MM3* the V2G charging scheme saves an additional 2.1% of the overall system costs compared to smart charging, much more than in the deterministic case. Consequently, the added system flexibility of a V2G charging scheme will become increasingly beneficial in the future, as we can expect more volatile renewable electricity supply and thus electricity prices.

V. Conclusion

We have analysed how different charging strategies for EV batteries, while considering battery degradation, affect overall system cost in the operational scheduling for a smart neighborhood in an urban setting.

The deterministic results show a reduction of charging costs by 10% through the change from passive charging to smart charging, due to the systems ability to shift the EV load to cheap price periods in the morning. Flexible charge pattern are not only beneficial to the whole neighborhood by reducing the peak load, grid dependency, and cost, but also for the individual EV owner by prolonging the EV life by 29%. With an added V2G option for the EVs the system costs reduce only 0.23%.

Uncertainty in electricity prices and EV arrival SOCs reveals a more significant improvement of V2G compared to smart charging. Due to the increased flexibility, the system can respond better to external changes. With the same price and SOC conditions as in the deterministic case, the V2G option is now 2.1% cheaper than passive charging. Consequently, the added system flexibility of a V2G charging scheme will become increasingly beneficial, as we can expect more volatile renewable production and thus electricity prices in the future.

We deduce five driver for V2G usage: *electricity price volatility*, *alternative energy sources*, *time of availability*, *departure SOC*, and *maximum charge and discharge power*.

Finally, we want to indicate model limitations and further research. The short optimization timeframe of one day leads to end of horizon issues, for which we had to introduce a penalty term in the objective and fix the stationary battery SOC to 30%. This fixed value takes variability away, which lowers the scenario variance for the battery in a stochastic setting. Hence, a longer optimization timeframe would lead to more natural stationary battery behavior, especially in the context of degradation. Additionally, we apply degradation, which alters the generation scheduling, only on battery systems. Further research on the impact of degradation for other generation units, such as a CHP, could lead to a similar system changes.

References

[1] H. Gabbar, *Smart energy grid engineering*, eng, First edition. Amsterdam, Netherlands, 2017, ISBN: 0-12-809232-7.

[2] M. Vadari, *Smart Grid Redefined : Transformation of the Electric Utility.* Ser. Artech House Titles in Power Engineering. 2018, ISBN: 9781630814762.

[3] P. D. Lund, J. Mikkola, and J. Ypyä, "Smart energy system design for large clean power schemes in urban areas," *Journal of Cleaner Production*, vol. 103, 2015, Carbon Emissions Reduction: Policies, Technologies, Monitoring, Assessment and Modeling.

[4] N. G. Paterakis, O. Erdinç, I. N. Pappi, A. G. Bakirtzis, and J. P. Catalão, "Coordinated operation of a neighborhood of smart households comprising electric vehicles, energy storage and distributed generation," *IEEE Transactions on smart grid*, vol. 7, no. 6, 2016.

[5] F. E. Aliabadi, K. Agbossou, S. Kelouwani, N. Henao, and S. S. Hosseini, "Coordination of smart home energy management systems in neighborhood areas: A systematic review," *IEEE Access*, 2021.

[6] S. Rafique, M. J. Hossain, M. S. H. Nizami, U. B. Irshad, and S. C. Mukhopadhyay, "Energy management systems for residential buildings with electric vehicles and distributed energy resources," *IEEE Access*, vol. 9, 2021.

[7] H. Fontenot and B. Dong, "Modeling and control of building-integrated microgrids for optimal energy management–a review," *Applied Energy*, vol. 254, 2019.

[8] F. Khavari, A. Badri, A. Zangeneh, and M. Shafiekhani, "A comparison of centralized and decentralized energy-management models of multi-microgrid systems," in *2017 Smart Grid Conference*, IEEE, 2017.

[9] E. Sarker, P. Halder, M. Seyedmahmoudian, *et al.*, "Progress on the demand side management in smart grid and optimization approaches," *International Journal of Energy Research*, vol. 45, no. 1, 2021.

[10] P. Kumar, G. S. Brar, and L. Singh, "Energy efficiency evaluation in commercial and residential buildings with demand side management: A review," in *2019 8th International Conference on Power Systems (ICPS)*, 2019.

[11] L. Gkatzikis, I. Koutsopoulos, and T. Salonidis, "The role of aggregators in smart grid demand response markets," *IEEE Journal on Selected Areas in Communications*, vol. 31, no. 7, 2013.

[12] G. Pulazza, C. Orozco, A. Borghetti, F. Tossani, and F. Napolitano, "Procurement cost minimization of an energy community with biogas, photovoltaic and storage units," in *2021 IEEE Madrid PowerTech*, 2021.

[13] K. Mahani, M. A. Jamali, S. D. Nazemi, and M. A. Jafari, "Economic and operational evaluation of pv and chp combined with energy storage systems considering energy and regulation markets," in *2020 IEEE Texas Power and Energy Conference (TPEC)*, 2020.

[14] C. Widmann, D. Lödige, A. Toradmal, and B. Thomas, "Enabling chp units for electricity production on demand by smart management of the thermal energy storage," *Applied Thermal Engineering*, vol. 114, 2017.

[15] A. Ghasemi, M. Banejad, M. Rahimiyan, and M. Zarif, "Investigation of the micro energy grid operation under energy price uncertainty with inclusion of electric vehicles," *Sustainable Operations and Computers*, vol. 2, 2021.

[16] N. Eghbali, S. M. Hakimi, A. Hasankhani, G. Derakhshan, and B. Abdi, "A scenario-based stochastic model for day-ahead energy management of a multi-carrier microgrid considering uncertainty of electric vehicles," *Journal of Energy Storage*, vol. 52, 2022.

[17] M. Alipour, B. Mohammadi-Ivatloo, and K. Zare, "Stochastic scheduling of renewable and chp-based microgrids," *IEEE Transactions on Industrial Informatics*, vol. 11, no. 5, 2015.

[18] H. Li, A. Rezvani, J. Hu, and K. Ohshima, "Optimal day-ahead scheduling of microgrid with hybrid electric vehicles using msfla algorithm considering control strategies," *Sustainable Cities and Society*, vol. 66, 2021.

[19] H. K. Nunna, S. Battula, S. Doolla, and D. Srinivasan, "Energy management in smart distribution systems with vehicle-to-grid integrated microgrids," *IEEE transactions on smart grid*, vol. 9, no. 5, 2016.

[20] Q. Guo, S. Nojavan, S. Lei, and X. Liang, "Economic-environmental analysis of renewable-based microgrid under a cvar-based two-stage stochastic model with efficient in-

tegration of plug-in electric vehicle and demand response," *Sustainable Cities and Society*, vol. 75, 2021.

[21] T. Ding, M. Qu, C. Huang, Z. Wang, P. Du, and M. Shahidehpour, "Multi-period active distribution network planning using multi-stage stochastic programming and nested decomposition by sddip," *IEEE Transactions on Power Systems*, vol. 36, no. 3, 2020.

[22] F. Hafiz, A. R. de Queiroz, P. Fajri, and I. Husain, "Energy management and optimal storage sizing for a shared community: A multi-stage stochastic programming approach," *Applied energy*, vol. 236, 2019.

[23] R. Lu, T. Ding, B. Qin, J. Ma, X. Fang, and Z. Dong, "Multi-stage stochastic programming to joint economic dispatch for energy and reserve with uncertain renewable energy," *IEEE Transactions on Sustainable Energy*, vol. 11, no. 3, 2019.

[24] W. H. Liu, S. R. W. Alwi, H. Hashim, *et al.*, "Optimal design and sizing of integrated centralized and decentralized energy systems," *Energy Procedia*, vol. 105, 2017.

[25] M. Rezaeimozafar, M. H. Amini, and M. Moradi, "Innovative appraisement of smart grid operation considering large-scale integration of electric vehicles enabling v2g and g2v systems," *Electric Power Systems Research*, vol. 154, Jan. 2018.

[26] D. Fischer, A. Harbrecht, A. Surmann, and R. McKenna, "Electric vehicles' impacts on residential electric local profiles – a stochastic modelling approach considering socio-economic, behavioural and spatial factors," *Applied Energy*, vol. 233-234, 2019.

[27] Y. Amara-Ouali, Y. Goude, P. Massart, J.-M. Poggi, and H. Yan, "A review of electric vehicle load open data and models," *Energies*, vol. 14, no. 8, 2021.

[28] A. Leippi, M. Fleschutz, and M. D. Murphy, "A review of ev battery utilization in demand response considering battery degradation in non-residential vehicle-to-grid scenarios," *Energies*, vol. 15, no. 9, 2022.

[29] A. Ahmadian, M. Sedghi, A. Elkamel, M. Fowler, and M. Aliakbar Golkar, "Plug-in electric vehicle batteries degradation modeling for smart grid studies: Review, assessment and conceptual framework," *Renewable and Sustainable Energy Reviews*, vol. 81, 2018.

[30] A. W. Thompson, "Economic implications of lithium ion battery degradation for vehicle-to-grid (v2x) services," *Journal of Power Sources*, vol. 396, 2018.

[31] P. Keil, S. F. Schuster, J. Wilhelm, *et al.*, "Calendar aging of lithium-ion batteries," *Journal of The Electrochemical Society*, vol. 163, no. 9, 2016.

[32] J. Yusuf and S. Ula, "A comprehensive optimization solution for buildings with distributed energy resources and v2g operation in smart grid applications," in *2020 IEEE Power Energy Society Innovative Smart Grid Technologies Conference (ISGT)*, 2020.

[33] M. Shakeri, M. Shayestegan, H. Abunima, *et al.*, "An intelligent system architecture in home energy management systems (hems) for efficient demand response in smart grid," *Energy and Buildings*, vol. 138, 2017.

[34] A. K. Erenoğlu, İ. Şengör, O. Erdinç, A. Taşcıkaraoğlu, and J. P. Catalão, "Optimal energy management system for microgrids considering energy storage, demand response and renewable power generation," *International Journal of Electrical Power & Energy Systems*, vol. 136, 2022.

[35] J. Silvente and L. G. Papageorgiou, "An milp formulation for the optimal management of microgrids with task interruptions," *Applied energy*, vol. 206, 2017.

[36] D. Thomas, O. Deblecker, and C. S. Ioakimidis, "Optimal operation of an energy management system for a grid-connected smart building considering photovoltaics' uncertainty and stochastic electric vehicles' driving schedule," *Applied Energy*, vol. 210, 2018.

[37] J. A. Pinzon, P. P. Vergara, L. C. Da Silva, and M. J. Rider, "Optimal management of energy consumption and comfort for smart buildings operating in a microgrid," *IEEE transactions on smart grid*, vol. 10, no. 3, 2018.

[38] K. Ginigeme and Z. Wang, "Distributed optimal vehicle-to-grid approaches with consideration of battery degradation cost under real-time pricing," *IEEE Access*, vol. 8, 2020.

[39] B. Xu, J. Zhao, T. Zheng, E. Litvinov, and D. S. Kirschen, "Factoring the cycle aging cost of batteries participating in electricity markets," *IEEE Transactions on Power Systems*, vol. 33, no. 2, 2018.

[40] S. Bjarghov, M. Kalantar-Neyestanaki, R. Cherkaoui, and H. Farahmand, "Battery Degradation-Aware Congestion Management in Local Flexibility Markets," in *2021 IEEE Madrid PowerTech*, 2021.

[41] K. Schwenk, S. Meisenbacher, B. Briegel, T. Harr, V. Hagenmeyer, and R. Mikut, "Integrating battery aging in the optimization for bidirectional charging of electric vehicles," *IEEE Transactions on Smart Grid*, vol. 12, no. 6, 2021.

[42] W. Vermeer, G. R. Chandra Mouli, and P. Bauer, "Real-time building smart charging system based on pv forecast and li-ion battery degradation," *Energies*, vol. 13, no. 13, 2020.

[43] C. Schade and R. Egging-Bratseth, "The impact of battery degradation on economic dispatch optimization, in review,"

[44] I. Laresgoiti, S. Käbitz, M. Ecker, and D. Sauer, "Modeling mechanical degradation in lithium ion batteries during cycling: Solid electrolyte interphase fracture," *Journal of Power Sources*, vol. 300, Dec. 2015.

[45] N. Hashemipour, P. Crespo del Granado, and J. Aghaei, "Dynamic allocation of peer-to-peer clusters in virtual local electricity markets: A marketplace for ev flexibility," *Energy*, vol. 236, 2021.

[46] "Gurobi optimization, llc. www.gurobi.com/products/gurobi-optimizer." (2021).

[47] "Xrgi20 technical data. www.ecpower.eu." ().

[48] A. Barfield. "Replacing the nissan leaf battery is insanely expensive." (2020), [Online]. Available: www.motorbiscuit.com/replacing-the-nissan-leaf-battery-is-insanely-expensive/.

[49] L. Mauler, F. Duffner, W. G. Zeier, and J. Leker, "Battery cost forecasting: A review of methods and results with an outlook to 2050," *Energy & Environmental Science*, 2021.

[50] B. Rumberg, B. Epding, I. Stradtmann, M. Schleder, and A. Kwade, "Holistic calendar aging model parametrization concept for lifetime prediction of graphite/nmc lithium-ion cells," *Journal of Energy Storage*, vol. 30, 2020.

[51] A. Krupp, R. Beckmann, T. Diekmann, E. Ferg, F. Schuldt, and C. Agert, "Calendar aging model for lithium-ion batteries considering the influence of cell characterization," *Journal of Energy Storage*, vol. 45, 2022.

[52] B. Xu, A. Oudalov, A. Ulbig, G. Andersson, and D. S. Kirschen, "Modeling of lithium-ion battery degradation for cell life assessment," *IEEE Transactions on Smart Grid*, vol. 9, no. 2, 2018.

[53] "Electricity price." (2019), [Online]. Available: strom-report.de/strompreise/#strompreiszusammensetzung.

[54] Eurostat. "Gas prices for household consumers - bi-annual data (from 2007 onwards)." (2019), [Online]. Available: https://ec.europa.eu/eurostat/databrowser/view/nrg_pc_202/default/table.

[55] BMWI. (), [Online]. Available: www.gesetze-im-internet.de/eeg_2014/__21.html.

Bibliography

[1] IPCC. *Climate Change 2022: Mitigation of Climate Change.* H.-O. Pörtner et al., 2022.

[2] Zihang Qiu et al. 'Charging rate based battery energy storage system model in wind farm and battery storage cooperation bidding problem'. In: *CSEE Journal of Power and Energy Systems* (2022), pp. 1–9.

[3] Jan Figgener et al. 'The development of stationary battery storage systems in Germany–status 2020'. In: *Journal of Energy Storage* 33 (2021), p. 101982.

[4] Yvenn Amara-Ouali et al. 'A Review of Electric Vehicle Load Open Data and Models'. In: *Energies* 14.8 (2021). ISSN: 1996-1073.

[5] Rui Xiong et al. 'Lithium-ion battery aging mechanisms and diagnosis method for automotive applications: Recent advances and perspectives'. In: *Renewable and Sustainable Energy Reviews* 131 (2020), p. 110048. ISSN: 1364-0321.

[6] Xuebing Han et al. 'A review on the key issues of the lithium ion battery degradation among the whole life cycle'. In: *eTransportation* 1 (2019), p. 100005. ISSN: 2590-1168.

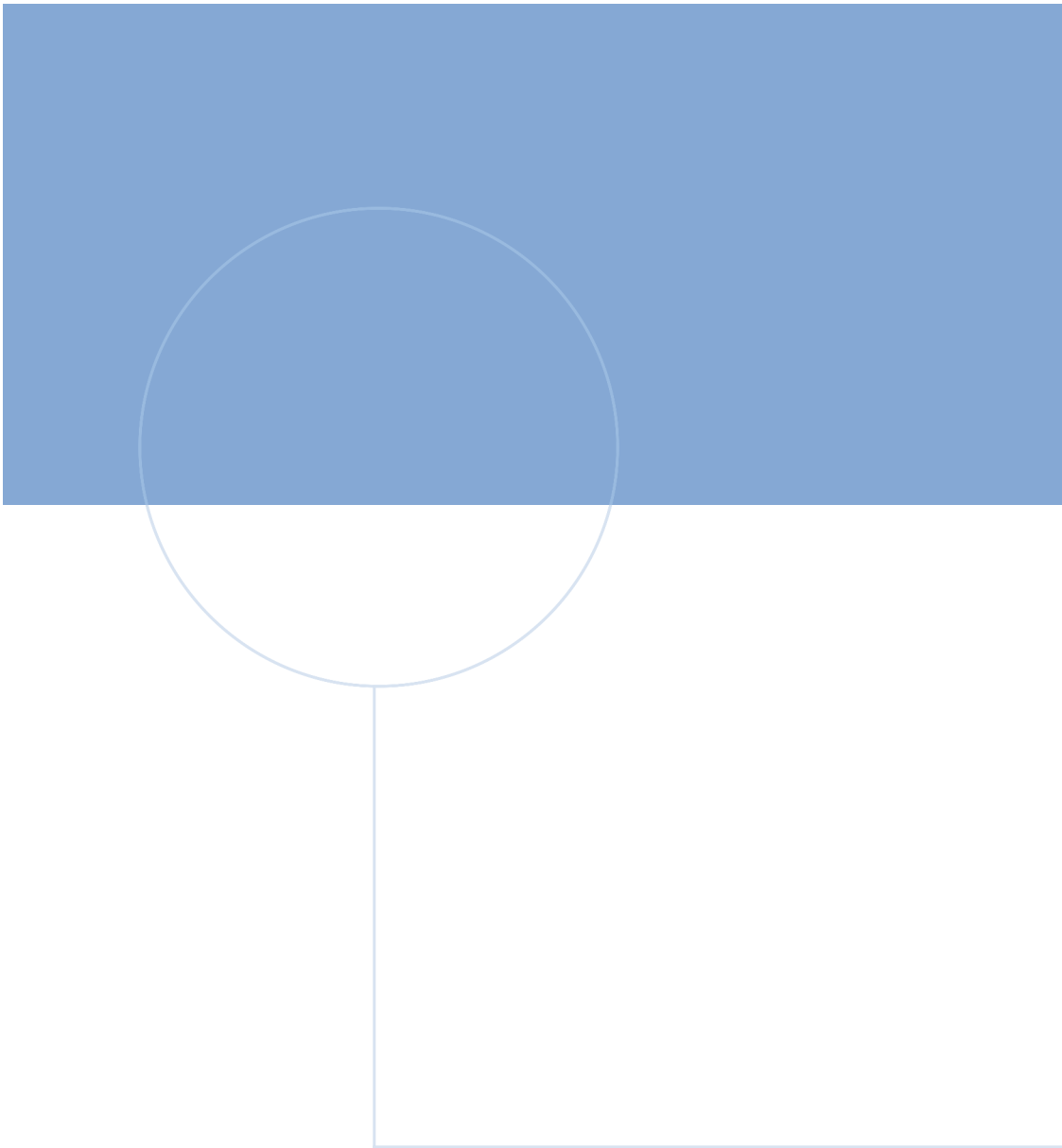

NTNU

Norwegian University of
Science and Technology